Arbitrary polynomial chaos expansion method for uncertainty quantification and global sensitivity analysis in structural dynamics

Hua-Ping Wan[a], Wei-Xin Ren[b], Michael D. Todd[c]

[a]*College of Civil Engineering and Architecture, Zhejiang University, Hangzhou 310058, China*

[b]*College of Civil and Transportation Engineering, Shenzhen University, Shenzhen 518060, China*

[c]*Department of Structural Engineering, University of California, San Diego, 9500 Gilman Dr. 0085, La Jolla, CA 92093-0085, USA*

Abstract: Uncertainty quantification (UQ) and global sensitivity analysis (GSA) of dynamic characteristics of complex systems subjected to uncertainty are jointly investigated in this paper. An efficient approach based on arbitrary polynomial chaos expansion (aPCE) is presented for analytical, unified implementation of UQ and GSA in structural dynamics. For UQ of dynamic characteristics, statistical moments and probability distributions of dynamic characteristics are analytically derived. Specifically, the aPCE is used to analytically calculate the statistical moments, and then the maximum entropy principle (MEP) is adopted to derive the closed-form expressions of the probability distributions using the obtained statistical moments. As an extension of UQ, GSA, which aims to assess the quantitative contributions of different structural parameters to the resultant variations of dynamic characteristics, is also analytically achieved by simply post-processing the aPCE coefficients. The present aPCE UQ and GSA method is highly computationally efficient for large-scale, complex structures, and it is also generally applicable independent of parameter

E-mail address: hpwan@zju.edu.cn (H.-P. Wan); renwx@szu.edu.cn (W.-X. Ren); mdtodd@eng.ucsd.edu (M. D. Todd).

distributions. The proposed aPCE-based approach for UQ and GSA is validated through a numerical truss bridge by the brute-force Monte Carlo simulation (MCS), and then is applied to a long-span steel arch bridge.

Keywords: Structural dynamics; Uncertainty quantification; Global sensitivity analysis; Arbitrary polynomial chaos expansion; Maximum entropy principle; Bridge structure.

1. Introduction

Our understanding of the dynamic behavior of structural and mechanical systems relies largely on representative computational (typically finite element) models that involve a large number of physical and geometric parameters such as material constants, stiffnesses, length, connectivity, and cross-sectional shape characteristics. Although the continuous development of more powerful and efficient computational capabilities allows for execution of very sophisticated and high-fidelity numerical models, it is common that these model-based predicted dynamic responses do not correlate well with the measured counterparts [1]. A variety of uncertainty sources exists associated with the structural model properties, including (but not limited to) manufacturing-induced tolerances, inherent random variation of materials, ill-defined boundary conditions, load variation, etc. These uncertainty sources are broadly classified into two categories, namely aleatory (also named stochastic, or irreducible, uncertainty resulting from inherent variation or randomness), and epistemic (also named subjective, or reducible uncertainty, due to lack of knowledge) [2].

Thus, the structural model parameters should be regarded as uncertain rather than deterministic, and in response the impact of uncertainty in structural parameters on structural dynamic characteristics is important to characterize. In recent years, uncertainty in

structural dynamics has received considerable attention from engineers as an active research branch [3, 4]. A surge of work has demonstrated that uncertainty quantification (UQ) and sensitivity analysis (SA) are two essential ingredients of quantitative uncertainty management of physical systems subjected to uncertainty [5]. UQ refers to evaluation of the uncertainty in model outputs propagated from the uncertainty in model inputs, whereas SA refers to the determination of the contributions of individual model inputs (or a subset of them) to the resultant variations of model outputs.

Specifically, the realization of UQ in linear structural dynamics is to quantify uncertainty in the eigencharacteristics (natural frequencies, mode shapes, and possibly damping) and frequency response functions in terms of confidence intervals, statistical moments, or probability distributions. There has been a large volume of work dedicated to this research direction, and a broad spectrum of UQ methods have been developed such as stochastic finite element method [6, 7], perturbation method [8, 9], interval analysis [10-13], surrogate modeling techniques [14-21], and Monte Carlo simulation (MCS) [1, 22]. On the other hand, comparatively little work has been conducted on SA in structural dynamics. The limited research work done on this area can be found in [23-25]. In general, SA techniques can be typically divided into two families, local and global. Local SA (LSA) measures effects of small variations of the model inputs in the vicinity of central (nominal) values through perturbing each single input slightly in turn while all other inputs are kept constant. In contrast to LSA, global SA (GSA), as its name indicates, assesses the impacts of the whole variations of the model inputs over their entire domain on model outputs. GSA is strongly recommended by researchers for performing SA of model output responses to uncertain model inputs, especially when the model under consideration is nonlinear, the

uncertainty level of model inputs is large, or interaction effects among model inputs cannot be ignored [26, 27]. In the literature, a variety of GSA techniques are available, including variance-based technique (e.g., Sobol method [28]), screening method (e.g., Morris method [29]), and regression method (e.g., standardized regression coefficients [30]), to name a few. Among them, the variance-based technique has been widely recognized as a powerful tool for reliable assessment of impacts of uncertain model inputs on model response. Thus, the variance-based GSA is the focus of this paper.

Of particular interest in this study is to conduct UQ and variance-based GSA together in structural dynamics. For large-scale complex structures, UQ and variance-based GSA can pose severe computational challenges, which will limit the applicability of traditional methods that are computationally expensive, such as MCS. For instance, the brute-force MCS implementation of UQ for a complex arch bridge run on a Dell desktop machine with Pentium (R) D CPU 2.80 GHz takes around 45 days (3.6×10^5 model evaluations) [17]. It should be noted that, with the MCS implementation, the computational cost of the variance-based GSA is several times higher than that of UQ because apart from estimation of the total variance, the variance-based GSA also has to compute a collection of partial variances arising from each parameter alone and the interaction effect with other parameters. In addition, the large-scale, complex structures (i.e., spacecraft, automobiles, bridges, and wind turbines) are commonly modeled as the high-resolution finite element (FE) models achieved by using commercial FE analysis packages, such as ANSYS and ABAQUS. This fact may exclude the use of the direct structural matrices (stiffness, mass, and damping matrices)-based UQ methods, such as the aforementioned perturbation method and interval analysis, since repeatedly extracting structural matrices from these FE analysis programs

and then conducting a series of calculations on these structural matrices for subsequent analysis is computationally prohibitive and thus impractical. In this circumstance, the surrogate modeling method can be seen as an effective tool for solving the issue of the high computational cost involved in UQ and variance-based GSA of dynamic characteristics of complex systems.

Polynomial chaos expansion (PCE) has received considerable attention recently in a wide range of applications [31-37], since it maintains great capability in modeling highly complex systems with a relatively low computational cost. PCE is a surrogate model to represent the probabilistic response as a series expansion of orthogonal polynomials of the input random variables. The PCE idea was originally proposed by Wiener [38] to model stochastic processes exclusively governed by Gaussian random variables. It was later extended by Xiu and Karniadakis [39] to a generalized PCE (gPCE) in which several classical probability distributions (i.e., Gamma, Beta, and uniform) specified random variables could be utilized. Most recently, PCE is further extended by Wan and Karniadakis [40] and Witteveen and Bijl [41] so that it can be suitable for modeling the arbitrary probability distributed random variables. This more generalized PCE is called *arbitrary* PCE (aPCE). Because of its substantial generality in dealing with arbitrary probability distributions, aPCE has been successfully applied to solve a wide range of engineering problems [42-46]. This paper proposes the use of aPCE for a unified implementation of UQ and variance-based GSA in structural dynamics. The main contributions of this study are threefold: (1) the implementation of aPCE, which enables to handle arbitrary probability distributions that are beyond these four aforementioned classical ones (i.e., Gaussian, Gamma, Beta, and uniform), is detailed; (2) UQ and variance-based GSA of dynamic

characteristics of complex systems are analytically implemented in a simultaneous fashion; and (3) for UQ consideration, in addition to the high-order statistical moments of dynamic characteristics, their probability distributions are also analytically derived by using maximum entropy principle (MEP). The present aPCE allows for generalizing the analytical implementation of UQ and variance-based GSA of stochastic dynamic systems with arbitrary probability distributed random variables. Although the applications in this paper are all structural dynamic problems, we stress that the aPCE approach is applicable to UQ and variance-based GSA of physical systems with arbitrary probability distributions in general.

2. Arbitrary polynomial chaos expansion

2.1. Formulation of arbitrary polynomial chaos expansion

Polynomial chaos expansion (PCE) is a spectral decomposition method that expands the model output to an infinite series of orthogonal polynomials in random model inputs. The arbitrary PCE (aPCE) is a generalized PCE that is suitable for the physical models whose input random variables are arbitrarily distributed. Assume $y=\mathcal{M}(\boldsymbol{\xi})$ is a physical model, which is usually an expensive-to-run black-box function, where $\boldsymbol{\xi}=\{\xi_1,\xi_2,\ldots,\xi_d\}$ is a collection of input random variables. Provided that the model output y has a finite variance, it can be written as an aPCE representation

$$\mathcal{M}(\boldsymbol{\xi})=\beta_0\Psi_0+\sum_{\alpha_1=1}^{d}\beta_{\alpha_1}\Psi_1(\xi_{\alpha_1})+\sum_{\alpha_1=1}^{d}\sum_{\alpha_2=1}^{\alpha_1}\beta_{\alpha_1\alpha_2}\Psi_2(\xi_{\alpha_1},\xi_{\alpha_2})+\sum_{\alpha_1=1}^{d}\sum_{\alpha_2=1}^{\alpha_1}\sum_{\alpha_3=1}^{\alpha_2}\beta_{\alpha_1\alpha_2\alpha_3}\Psi_3(\xi_{\alpha_1},\xi_{\alpha_2},\xi_{\alpha_3})+\cdots \quad (1)$$

or in a compact form

$$\mathcal{M}(\boldsymbol{\xi})=\sum_{\theta\in\mathbb{N}^d}\beta_\theta\Psi_\theta(\boldsymbol{\xi}) \quad (2)$$

where the multi-dimensional indices θ's are d-tuples in $\mathbb{N}^d$; β_θ are the PCE coefficients; and $\Psi_\theta(\boldsymbol{\xi})$ are the basis functions belonging to the Askey scheme of orthogonal polynomials, satisfying

$$\langle \Psi_m(\boldsymbol{\xi}), \Psi_n(\boldsymbol{\xi}) \rangle = \langle \Psi_m^2(\boldsymbol{\xi}) \rangle \delta_{mn} \tag{3}$$

where δ_{mn} represents the Kronecker delta that is one if $m = n$ and zero otherwise; and $\langle \bullet, \bullet \rangle$ defines the inner product

$$\langle \Psi_m(\boldsymbol{\xi}), \Psi_n(\boldsymbol{\xi}) \rangle = \mathbb{E}\left(\Psi_m(\boldsymbol{\xi}) \Psi_n(\boldsymbol{\xi})\right) = \int \Psi_m(\boldsymbol{\xi}) \Psi_n(\boldsymbol{\xi}) \, p(\boldsymbol{\xi}) d\boldsymbol{\xi} \tag{4}$$

where $\mathbb{E}(\bullet)$ stands for the expectation operator; and $p(\bullet)$ denotes the PDF.

The basis functions $\Psi_\theta(\boldsymbol{\xi})$ are multivariate polynomials constructed by tensor product of their univariate counterparts

$$\Psi_\theta(\boldsymbol{\xi}) = \prod_{i=1}^{d} \psi_{\theta_i}(\xi_i) \tag{5}$$

where the subscript θ_i refers to the i-th degree of the θ-th univariate polynomial basis; and $\psi_{\theta_i}(\xi_i)$ is univariate polynomials orthogonal with respect to the probability distribution $p(\xi_i)$.

In practice, the aPCE representation of the model response is truncated such that the total degree does not exceed the finite degree r, expressed as

$$\mathcal{M}(\boldsymbol{\xi}) \approx \sum_{\theta \in \mathcal{A}^{p,d}} \beta_\theta \Psi_\theta(\mathbf{x}), \quad \mathcal{A}^{p,d} \equiv \{\theta \in \mathbb{N}^d : \| \theta \|_1 \leq r\}. \tag{6}$$

This leads to the total number of terms in the truncated aPCE equal to

$$K + 1 = \binom{d + r}{d} = \frac{(d + r)!}{d! r!}, \tag{7}$$

where K represents the number of polynomials.

The methods for computation of the aPCE coefficients can be either intrusive or non-intrusive [47]. Since we often encounter physical models that are highly complicated

and only available as a black-box, the non-intrusive schemes are of our interest. Two non-intrusive solutions are the least-square estimator and the non-intrusive spectral projection (NISP) route. The latter may become impractical when the input dimensionality is high and the model is expensive. In such situation, the regression method is more effective. Let $\{\boldsymbol{\xi}_i\}\big|_{i=1}^{N}$ be N samples of random variables, known as the experimental design, which is usually implemented by the space-filling sampling schemes, such as Latin hypercube sampling (LHS) and quasi-random Sobol sequence. Then the original model solver is executed at each sample point to collect the corresponding target responses $\{y_i = \mathcal{M}(\boldsymbol{\xi}_i)\}\big|_{i=1}^{N}$. The determination of the aPCE coefficients involves solving the minimization problem of the ℓ_2-norm of the residual

$$\hat{\boldsymbol{\beta}}_\theta = \arg\min_{\beta_\theta \in \mathbb{N}^{K+1}} \sum_{i=1}^{N} \left(y_i - \sum_{\theta \in \mathcal{A}^{p,d}} \beta_\theta \psi_\theta(\boldsymbol{\xi}_i) \right)^2 . \tag{8}$$

Denoting

$$\mathbf{H} = \begin{bmatrix} \psi_0(\boldsymbol{\xi}_1) & \psi_1(\boldsymbol{\xi}_1) & \cdots & \psi_K(\boldsymbol{\xi}_1) \\ \psi_0(\boldsymbol{\xi}_2) & \psi_1(\boldsymbol{\xi}_2) & \cdots & \psi_K(\boldsymbol{\xi}_2) \\ \vdots & \vdots & \ddots & \vdots \\ \psi_0(\boldsymbol{\xi}_N) & \psi_1(\boldsymbol{\xi}_N) & \cdots & \psi_K(\boldsymbol{\xi}_N) \end{bmatrix}, \mathbf{y} = \begin{bmatrix} y_1 \\ y_2 \\ \vdots \\ y_N \end{bmatrix}, \tag{9}$$

the well-known least square solution of Eq. (8) is

$$\hat{\boldsymbol{\beta}}_\theta = (\mathbf{H}^\top \mathbf{H})^{-1} \mathbf{H}^\top \mathbf{y} . \tag{10}$$

2.2. Construction of univariate orthogonal polynomials

The aPCE is a sum of a finite set of multivariate polynomials $\Psi_\theta(\boldsymbol{\xi})$ that are formulated by the univariate orthogonal polynomials, and the univariate orthogonal polynomials $\psi_{\theta_i}(\xi_i)$ depend on the distribution type of the i-th random variable ξ_i. Therefore, the fundamental of formulating aPCE is to construct the arbitrary univariate orthogonal polynomials, which satisfy the well-known three-term recurrence relation [48]

$$\begin{aligned} \psi_{i+1}(\xi) &= (\xi - a_i)\psi_i(\xi) - b_i\psi_{i-1}, i = 0,1,2,\ldots \\ \psi_{-1}(\xi) &= 0,\ \psi_0(\xi) = 1 \end{aligned} . \tag{11}$$

with the recurrence coefficients determined by

$$a_i = \frac{\langle \xi\psi_i, \psi_i \rangle}{\langle \psi_i, \psi_i \rangle} \quad i = 0,1,2,\ldots. \tag{12}$$

$$b_i = \begin{cases} \langle \psi_0, \psi_0 \rangle & i = 0, \\ \dfrac{\langle \psi_i, \psi_i \rangle}{\langle \psi_{i-1}, \psi_{i-1} \rangle} & i = 1,2,\ldots. \end{cases} \tag{13}$$

uniquely determined by probability distribution $p(\xi)$.

2.3. Calculation of recurrence coefficients

The key to formulating univariate orthogonal polynomials is to calculate the recurrence coefficients. Although several standard probability distributions (e.g., normal, uniform, and Gamma) have analytical recurrence coefficients [44, 49], there exist many commonly-used probability distributions (e.g., Lévy, Weibull, and Chi-square) without exact recurrence coefficients. Therefore, there is a strong demand for finding the effective technique to compute the recurrence coefficients $\{a_i, b_i\}_{i=0}^{n-1}$ associated with arbitrary probability distributions.

The Moment-based method and the Stieltjes procedure are two classical approaches for calculation of the recurrence coefficients. The moment-based method uses the fact that the recurrence coefficients are explicitly expressed as the ratio of the Hankel determinants consisting of moments of probability distribution $p(\xi)$. More details about the moment-based method can be found in [48]. Unfortunately, the moment-based method is numerically problematic since it gives rise to the issue of the severe ill-conditioning. As a result, the moment-based method is not recommended as a method for calculating the recurrence coefficients [48]. The Stieltjes procedure is a method that evaluates the

recurrence coefficients in an iterative fashion, forming the sequence

$$\{\psi_0\}\to\{a_0,b_0\}\to\{\psi_1\}\to\{a_1,b_1\}\to\cdots\to\{\psi_{n-2}\}\to\{a_{n-1},b_{n-1}\}. \tag{14}$$

The Stieltjes procedure, however, also tends to be unstable, since the solution of the resultant set of algebraic equations for the recurrence coefficients in terms of moments of probability distribution $p(\xi)$ can be severely ill-conditioned [48]. Apart from the demerit of the numerical instability, for some measures $p(\xi)$, the classical two methods fail to compute the high-order Gaussian quadrature rules with enough precision [50].

The discretization method is widely recognized as a general-purpose and unconditionally stable scheme that is effective for calculating the recurrence coefficients associated with arbitrary probability distribution and the numerical comparison of these two procedures (Stieltjes and moment-based ones) and the discretization method is detailed in [48, 50]. The fundamental idea underlying the discretization approach is that the given continuous measure can be approximated by a discrete n-point measure with the form of

$$\omega_n(\xi)=\sum_{i=1}^{n}\omega_i\delta\left(\xi-\xi_i\right). \tag{15}$$

With the nodes ξ_i and weights ω_i, we form the vector $\sqrt{\boldsymbol{\omega}}$ and diagonal matrix $\mathbf{D}$ defined by

$$\sqrt{\boldsymbol{\omega}}=\begin{bmatrix}\sqrt{\omega_1}\\ \sqrt{\omega_2}\\ \vdots\\ \sqrt{\omega_n}\end{bmatrix},\mathbf{D}=\begin{bmatrix}\xi_1 & & & \\ & \xi_2 & & \\ & & \ddots & \\ & & & \xi_n\end{bmatrix} \tag{16}$$

Then, it exists an orthogonal matrix $\mathbf{Q}_1$ such that [48]

$$\begin{bmatrix}1 & \mathbf{0}^{\top}\\ \mathbf{0} & \mathbf{Q}_1^{\top}\end{bmatrix}\begin{bmatrix}1 & \sqrt{\boldsymbol{\omega}}^{\top}\\ \sqrt{\boldsymbol{\omega}} & \mathbf{D}\end{bmatrix}\begin{bmatrix}1 & \mathbf{0}^{\top}\\ \mathbf{0} & \mathbf{Q}_1\end{bmatrix}=\begin{bmatrix}1 & \sqrt{b_0}\,\mathbf{e}^{\top}\\ \sqrt{b_0}\,\mathbf{e} & \mathbf{J}_1\end{bmatrix} \tag{17}$$

where $\mathbf{e}^{\top}=[1,0,\ldots,0]_{1\times n}$ and $\mathbf{J}_1$ is the Jacobi matrix associated with $p(\xi)$, expressed by

$$\mathbf{J}_1=\begin{bmatrix} a_0 & \sqrt{b_1} & & & \\ \sqrt{b_1} & a_1 & \sqrt{b_2} & & \\ & \sqrt{b_2} & \ddots & \ddots & \\ & & \ddots & a_{n-2} & \sqrt{b_{n-1}} \\ & & & \sqrt{b_{n-1}} & a_{n-1} \end{bmatrix}. \tag{18}$$

Eq. (17) is the expression of an orthogonal similarity transformation, written in a general form

$$\mathbf{Q}^{\top}\mathbf{A}\mathbf{Q}=\mathbf{J} \tag{19}$$

with

$$\mathbf{Q}=\begin{bmatrix} 1 & \mathbf{0}^{\top} \\ \mathbf{0} & \mathbf{Q}_1^{\top} \end{bmatrix},\ \mathbf{A}=\begin{bmatrix} 1 & \sqrt{\boldsymbol{\omega}}^{\top} \\ \sqrt{\boldsymbol{\omega}} & \mathbf{D} \end{bmatrix},\ \mathbf{J}=\begin{bmatrix} 1 & \sqrt{b_0}\,\mathbf{e}^{\top} \\ \sqrt{b_0}\,\mathbf{e} & \mathbf{J}_1 \end{bmatrix} \tag{20}$$

where $\mathbf{J}$ is the "extended" Jacobi matrix. The orthogonal matrix $\mathbf{Q}$ and the "extended" Jacobi matrix $\mathbf{J}$ are uniquely determined by $\mathbf{A}$ and the first column of $\mathbf{Q}$ [51].

Apparently, the weights ω_i and abscissae ξ_i with respect to the discrete measure $\omega_n(\xi)$ are the basis of the determination of the recurrence coefficients. The core of calculating $\{\omega_i,\xi_i\}|_{i=1}^{n}$ is to select a sequence of measures that are able to converge to the measure $p(\xi)d\xi$. Herein, we adopt the fast Fejér Type-2 integration scheme, which can be efficiently implemented by the inverse fast Fourier transform. Fejér Type-2 rules are very similar to the well-known Clenshaw-Curtis ones with the support $[-1,1]$, but Fejér Type-2 rules are open-ended, which makes them more suitable for measures with non-compact support. To use the fast Fejér Type-2 integration for $\omega(\xi)$ with an arbitrary domain [*l*, u] (*l* and *u* may be either finite or infinite), a suitable transformation scheme can be adopted to scale [*l*, u] into the interval [-1, 1], expressed as

$$\int_l^u \omega(\xi)dx = \int_{-1}^{1} \omega\big(\phi(\tau)\big)\phi'(\tau)d\tau \tag{21}$$

where the transformation function $\phi(\tau)$ is given by [48]

$$\phi(\tau) = \begin{cases} \dfrac{u-l}{2}\tau + \dfrac{u+l}{2} & \text{if } -\infty < l < u < \infty \\ u - \dfrac{1-\tau}{1+\tau} & \text{if } -\infty = l < u < \infty \\ l + \dfrac{1+\tau}{1-\tau} & \text{if } -\infty < l < u = \infty \\ \dfrac{\tau}{1-\tau^2} & \text{if } -\infty = l < u = \infty \end{cases}, \tag{22}$$

and its derivative is given by

$$\phi'(\tau) = \begin{cases} \dfrac{u-l}{2} & \text{if } -\infty < l < u < \infty \\ \dfrac{2}{(1+\tau)^2} & \text{if } -\infty = l < u < \infty \\ \dfrac{2}{(1-\tau)^2} & \text{if } -\infty < l < u = \infty \\ \dfrac{1+\tau^2}{\left(1-\tau^2\right)^2} & \text{if } -\infty = l < u = \infty \end{cases}. \tag{23}$$

Subsequently, the abscissae and weights in Eq. (15) are obtained from

$$\begin{aligned} \xi_i &= \phi(z_i) \\ \omega_i &= q_i\,\omega(z_i)\phi'(z_i) \end{aligned} \tag{24}$$

where $\{z_i, q_i\}$ are the abscissae and weights of the Fejér Type-2 rules. The expressions of the nodes and the weights of the Fejér Type-2 rules are given in Appendix A.

Once we obtain the abscissae and weights $\{\omega_i, \xi_i\}\big|_{i=1}^{n}$, the recurrence coefficients can be obtained by the orthogonal similarity transformation. Since the traditional Lanczos algorithm is numerically unstable, Givens rotation technique developed by Gragg and Harrod [52] is utilized to perform the orthogonal similarity transformation. The implementation details about conducting the orthogonal similarity transformation ($\mathbf{A} \to \mathbf{J}$) are given in their pseudocode RKPW algorithm. Finally, the recurrence coefficients included

in the "extended" Jacobi matrix $\mathbf{J}$ are obtained. To ensure the high accuracy in the recurrence coefficients, they are computed iteratively using the following stopping criterion [53]

$$|b_i^s - b_i^{s-1}| \le \varepsilon b_i^s, \quad i = 1,2,\ldots,n, \tag{25}$$

where s is the iteration step; and ε is the defined error tolerance (say 10^{-13}). A flowchart outlining the computational procedures of the recurrence coefficients is given in Fig. 1.

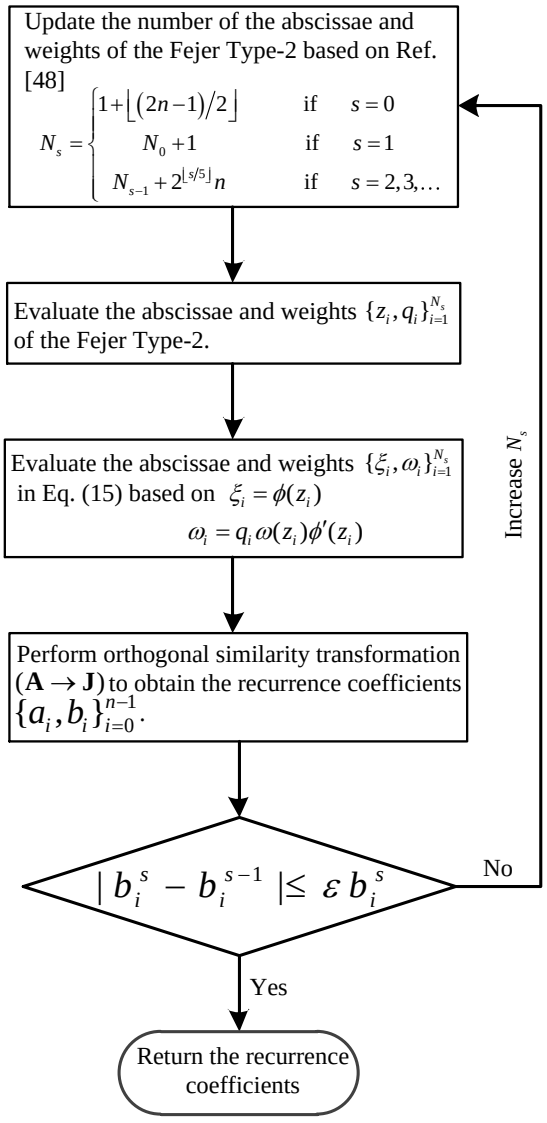

Figure 1. Flowchart of calculation of recurrence coefficients.

2.4. Model validation

The model validation process should be carried out to check the predictive capability of the constructed aPCE before being applied for subsequent analyses. In this study, the well-known leave-one-out cross-validation (LOOCV) is adopted for model diagnosis. LOOCV takes a single data point from the entire data set as the test data, and then the remaining data points are used as training data for building the aPCE. This LOOCV procedure is repeated such that each of data points is used once for validation, and the validation error-specific measure criterion is utilized for model validation.

The error at *i*-th data point $\boldsymbol{\xi}_i$ between the model evaluation and the aPCE prediction is

$$\Delta_i = \mathcal{M}(\boldsymbol{\xi}_i) - \hat{\mathcal{M}}_{-\boldsymbol{\xi}_i}(\boldsymbol{\xi}_i), \tag{26}$$

where $\mathcal{M}(\boldsymbol{\xi}_i)$ is the model evaluation; and $\hat{\mathcal{M}}_{-\boldsymbol{\xi}_i}(\boldsymbol{\xi}_i)$ is the aPCE prediction using the entire data set excluding the data point $\boldsymbol{\xi}_i$. The corresponding generalization leave-one-out (LOO) error is then estimated by the mean predicted residual sum of squares [54]

$$Err_{\mathrm{LOO}} = \frac{1}{N}\sum_{i=1}^{N}\Delta_i^2 . \tag{27}$$

The standardized LOO error is given by

$$\varepsilon_{\mathrm{LOO}} = \frac{Err_{\mathrm{LOO}}}{\mathbb{V}(y)}, \tag{28}$$

and the measure criterion associated with the LOOCV is defined as

$$Q^2 = 1 - \varepsilon_{\mathrm{LOO}} . \tag{29}$$

The larger the value of Q^2, the more accurate the constructed aPCE. Here, a threshold of 0.95 is used to determine whether the predictive quality of the aPCE is satisfactory or not.

3. Uncertainty quantification and global sensitivity analysis by aPCE

3.1. Uncertainty quantification

Uncertainty quantification (UQ) is the process of estimating metrics of uncertainty in quantities of interest that derives from uncertainty in model inputs. UQ is usually done in a probabilistic framework, in which the input uncertainties are parameterized by random variables following specific probability distribution functions (PDFs), and the resultant response uncertainties are characterized with probabilistic characteristics, such as statistical moments, confidence intervals, and PDF. Among these probabilistic features, PDF is the most valuable quantity since it contains the most substantial information for characterizing the response uncertainty. Once we obtain the PDFs of responses, other probabilistic characteristics can be readily calculated. Traditionally, the PDF is estimated from a large number of model evaluations by MCS procedure; however, this leads to the issue of high computational cost. In this section, we propose the aPCE-based approach for efficiently estimating the PDFs of responses. Specifically, the aPCE is proposed for analytical calculation of fundamental moments of responses, and then maximum entropy principle is utilized to infer their PDFs in light of the obtained moments.

3.1.1. Analytical calculation of fundamental moments

The aPCE is used to map the input-output relationship of the target model $y = \mathcal{M}(\boldsymbol{\xi})$. Therefore, according to probability theory, the moments of the aPCE-derived responses can be written as

$$\mu_y^k = \int \mathcal{M}^k(\boldsymbol{\xi}) p(\boldsymbol{\xi}) d\boldsymbol{\xi} \approx \int \left(\sum_{\boldsymbol{\alpha} \in \mathbb{N}^d} \beta_{\boldsymbol{\alpha}} \Psi_{\boldsymbol{\alpha}}(\boldsymbol{\xi}) \right)^k p(\boldsymbol{\xi}) d\boldsymbol{\xi}, \tag{30}$$

where μ_y^k denotes the k-th moment.

By applying the orthogonal identities of multivariate polynomials of aPCE, the analytical expressions of the first- and second-order moments can be attained as follows

$$\mu_y^1 = \beta_0 \tag{31}$$

$$\mu_y^2 = \sum_{i=0}^{K} \beta_i^2 \,. \tag{32}$$

Unlike the first two order moments, the high-order ones do not have compact expressions since the higher powers of aPCE become complex. Since aPCE is a polynomial function with the random variables of all the terms being separable, its powers are also polynomials with separable random variables. Due to this fact, the higher-order moments of model responses can be finally expressed in terms of the moments of univariate distributions associated with input random variables, written as

$$\mu_y^k = f_k(\mu_{\xi_1}, \mu_{\xi_2}, \ldots, \mu_{\xi_d}) \tag{33}$$

where $f_k(\bullet)$ is the simplest forms of the k-th power of the aPCE; and μ_{ξ_i} is the moment of the i-th input random variable.

Therefore, the use of the aPCE enables the analytical calculations of the fundamental moments of the model outputs, i.e., the moments of the model outputs are finally converted to simply post-processing the aPCE coefficients and moments of input random variables. In this regard, the analytical expressions of moments of input random variables will lead to analytical calculation of moments of the model outputs. Fortunately, most widely-used standard probability distributions have analytical expressions of the moments, which are provided in Appendix B. The resultant moments of the responses will serve as the basis for inferring their PDFs by using the maximum entropy principle.

3.1.2. Estimation of probability distribution by the maximum entropy principle

The idea behind the maximum entropy principle (MEP) [55] is that the most unbiased probability distribution of a random variable is the one that maximizes the Shannon entropy subjected to constraints supplied by the available information, e.g., a random variable's

297 statistical moments. The MEP provides a particularly useful tool for PDF characterization
298 since generally the statistical moments of a random variable can be achieved more easily
299 than its probability distribution. Let model output y be a random variable, and the entropy
300 of its PDF $p(y)$ can be expressed as

$$H = -\int p(y)\ln p(y)dy. \tag{34}$$

301 According to the MEP, the best probability distribution is the one with maximal
302 entropy, which comes up with an optimization problem below

$$\begin{aligned} &\text{maximize} \quad H = -\int p(y)\ln p(y)dy \\ &\text{s.t.} \quad \mathbb{E}\left(\phi_j(y)\right) = \int \phi_j(y)\,p(y)dy = \mu_\phi^j, \;\; j = 0,1,\ldots,m \end{aligned} \tag{35}$$

303 where $\phi_j(y)$ denotes the basis function associated with the moment constraints and
304 $\phi_0(y) = 1, \mu_0 = 1$. In this study, the geometrical moments of the model output y are taken
305 as the constraints of the optimization problem, so the constraint conditions become

$$\mathbb{E}(y^j) = \int y^j p(y)dy = \mu_y^j, \;\; j = 0,1,\ldots,m. \tag{36}$$

306 The above optimization problem defined in Eq. (35) can be solved by introducing
307 Lagrangian function, expressed as

$$L(p(y),\boldsymbol{\lambda}) = -\int p(y)\ln p(y)dy - \sum_{j=0}^{m}\lambda_j\left(\int y^j p(y)dy - \mu_y^j\right) \tag{37}$$

308 where $\boldsymbol{\lambda} = [\lambda_1,\ldots,\lambda_m]$ are the Lagrangian multipliers. Then the optimization problem is
309 reduced to solving the maximum of the Lagrangian function under the following constraints

$$\frac{\partial L(p(y),\boldsymbol{\lambda})}{\partial p(y)} = \int\left(-1-\ln p(y) - \sum_{j=0}^{m}\lambda_j y^j\right)dy = 0. \tag{38}$$

310 Finally, the solution of the optimization problem defined with the spirit of MEP leads to a
311 closed-form expression of PDF, given as

$$p(y) = \exp\left(-1-\sum_{j=0}^{m}\lambda_j y^j\right). \tag{39}$$

The Lagrangian multipliers $\boldsymbol{\lambda}$ can be determined by using the constraint conditions given in Eq. (36). It becomes the solution of multiple nonlinear equations below

$$\prod_m(\boldsymbol{\lambda}) = \int y^j \exp\left(-1-\sum_{j=0}^{m}\lambda_j y^j\right)dy = \mu_y^j,\ \ j=0,1,\ldots,m. \tag{40}$$

In general, these equations can be effectively solved by the standard Newton-Raphson method that is an iterative method for finding the roots of a differentiable function. Specifically, it starts with expanding objective function in Taylor series around an initial guess of the unknown parameters dropping terms of order higher than linear, and then solves the resulting linear system iteratively. The first-order Taylor series expansion of the objective function $\prod(\boldsymbol{\lambda})$ around an initial guess $\boldsymbol{\lambda}_0$ is

$$\prod_m(\boldsymbol{\lambda}) \cong \prod_m(\boldsymbol{\lambda}_0) + (\boldsymbol{\lambda}-\boldsymbol{\lambda}_0)\left.\frac{\partial \prod_m(\boldsymbol{\lambda})}{\partial \boldsymbol{\lambda}}\right|_{\boldsymbol{\lambda}=\boldsymbol{\lambda}_0}. \tag{41}$$

Combining Eqs. (40) and (41), one has

$$\boldsymbol{G}\boldsymbol{\delta} = \boldsymbol{\nu} \tag{42}$$

with

$$\begin{aligned}
\boldsymbol{\delta} &= (\boldsymbol{\lambda}-\boldsymbol{\lambda}_0)^{\top} \\
\boldsymbol{\nu} &= \left[\mu_y^0 - \prod_0(\boldsymbol{\lambda}_0), \cdots,\ \mu_y^m - \prod_m(\boldsymbol{\lambda}_0)\right]^{\top} \\
\boldsymbol{G} &= \left[\begin{array}{cccc}
\frac{\partial \prod_0(\boldsymbol{\lambda})}{\partial \lambda_0} & \frac{\partial \prod_0(\boldsymbol{\lambda})}{\partial \lambda_1} & \cdots & \frac{\partial \prod_0(\boldsymbol{\lambda})}{\partial \lambda_m} \\
\frac{\partial \prod_1(\boldsymbol{\lambda})}{\partial \lambda_0} & \frac{\partial \prod_1(\boldsymbol{\lambda})}{\partial \lambda_1} & \cdots & \frac{\partial \prod_1(\boldsymbol{\lambda})}{\partial \lambda_m} \\
\vdots & \vdots & \ddots & \vdots \\
\frac{\partial \prod_m(\boldsymbol{\lambda})}{\partial \lambda_0} & \frac{\partial \prod_m(\boldsymbol{\lambda})}{\partial \lambda_1} & \cdots & \frac{\partial \prod_m(\boldsymbol{\lambda})}{\partial \lambda_m}
\end{array}\right]_{\boldsymbol{\lambda}=\boldsymbol{\lambda}_0}
\end{aligned} \tag{43}$$

where $\boldsymbol{G}_{pq} = \dfrac{\partial \prod_p(\boldsymbol{\lambda})}{\partial \lambda_q} = -\int y^p y^q \exp\left(-1-\sum_{j=0}^{m}\lambda_j y^j\right)dy = -\prod_{p+q}(\boldsymbol{\lambda})$.

The linear equation Eq. (42) is solved for the perturbation $\boldsymbol{\delta}$ to determine the new initial guess $\boldsymbol{\lambda}=\boldsymbol{\lambda}_0+\boldsymbol{\delta}$. The iteration process will continue until the perturbation $\boldsymbol{\delta}$

becomes substantially smaller, and the final solution of $\boldsymbol{\lambda}$ is obtained. Eventually, the closed-form expression of PDF can be readily attained based on Eq. (39).

3.2. Variance-based global sensitivity analysis

Variance-based GSA is to quantify the contributions of individual parameters or parameter groups to the variance of the model output of interest. The fundamental philosophy of variance-based GSA is the functional analysis of variance (ANOVA) that the total variance of the model output can be decomposed into a collection of partial variances attributed to the main effects of individual inputs as well as their interaction effects. The decomposition of the total variance of model output $y = \mathcal{M}(\boldsymbol{\xi})$ into partial variances has the following form [28]

$$V = \sum_{1\le i\le d} V_i + \sum_{1\le i<j\le d} V_{i,j} + \sum_{1\le i<j<k\le d} V_{i,j,k} + \cdots + V_{1,2,\ldots,d} \tag{44}$$

where

$$\begin{aligned} V &= \mathbb{V}(y) \\ V_i &= \mathbb{V}(\mathbb{E}(y \mid \xi_i)) \\ V_{i,j} &= \mathbb{V}(\mathbb{E}(y \mid \boldsymbol{\xi}_{i,j})) - V_i - V_j \\ V_{i,j,k} &= \mathbb{V}(\mathbb{E}(y \mid \boldsymbol{\xi}_{i,j,k})) - V_{i,j} - V_{i,k} - V_{j,k} - V_i - V_j - V_k \\ &\cdots \end{aligned} \tag{45}$$

in which ξ_i is single input; $\boldsymbol{\xi}_{i,j}$ is input set of ξ_i and ξ_j; $\boldsymbol{\xi}_{i,j,k}$ is input set of ξ_i, ξ_j and ξ_k; and $\mathbb{E}(\bullet)$ and $\mathbb{V}(\bullet)$ denote the expectation and variance operators, respectively.

Normalizing the partial variances by the total variance V leads to the fractional contribution to the variance of each input, which are named as the variance-based sensitivity indices

$$S_u = \frac{V_u}{V} \in [0,1] \tag{46}$$

where subscript $u \subseteq \{1,2,\ldots,\mathrm{d}\}, u \neq \varnothing$. Apparently, all sensitivity indices sum up to one

$$\sum_{1\le i\le d} S_i + \sum_{1\le i<j\le d} S_{i,j} + \sum_{1\le i<j<k\le d} S_{i,j,k} + \cdots + S_{1,2,\ldots,d} = 1. \tag{47}$$

The first-order sensitivity index S_i assesses the amount of partial variance accounted for by x_i alone; the second-order sensitivity index $S_{i,j}$ measures the amount of partial variance due to the interaction effect of x_i and x_j; and the higher order sensitivity index $S_{i,j,\ldots,p}$ quantifies the joint influences from larger sets of inputs. In this sense, the total sensitivity index, which evaluates the total effect of single input, is defined as

$$S_{Ti} = \sum_{v:i\in v} S_v, \tag{48}$$

where v are all the subsets of indices including index i. For example, in the case of a model with 3 inputs, we have $S_{T1} = S_1 + S_{1,2} + S_{1,3} + S_{1,2,3}$.

When the system under consideration has a large number of inputs, the computation of total sensitivity index S_{Ti} using Eq. (48) is daunting. In this situation, one can resort to a more simplified expression in the form

$$S_{Ti} = 1 - \frac{V_{-i}}{V} \tag{49}$$

where $V_{-i} = \mathbb{V}(\mathbb{E}(y \mid \boldsymbol{\xi}_{-i}))$, in which $\boldsymbol{\xi}_{-i}$ indicates the set of all inputs except ξ_i.

Variance-based GSA is a powerful and robust means for assessment of the relative importance of inputs since it accounts for the effects of the entire parameter variation and interaction effects on the model output. However, the main difficulty encountered when performing variance-based GSA of the expensive-to-run physical model is a huge number of model executions required, which excludes the traditional MCS estimator. To address the problem of the high computational cost, the computationally cheap surrogate models are widely adopted in GSA community. Owing to the orthogonal nature of the basis functions of aPCE, the sensitivity indices can be calculated analytically [47, 56]. To be specific, the

variance-based sensitivity indices can be readily attained by post-processing aPCE coefficients, such that

$$\hat{S}_i = \frac{\sum_{k\in\mathcal{L}_i} \beta_k^2 \langle \psi_k, \psi_k \rangle}{\sum_{k=1}^{K} \beta_k^2 \langle \psi_k, \psi_k \rangle} \tag{50}$$

$$\hat{S}_{Ti} = \frac{\sum_{k\in\mathcal{K}_{Ti}} \beta_k^2 \langle \psi_k, \psi_k \rangle}{\sum_{k=1}^{K} \beta_k^2 \langle \psi_k, \psi_k \rangle} \tag{51}$$

where index sets $\mathcal{L}_i = \{k \in \mathcal{A}^{p,d} : k_i > 0, k_\ell = 0, \ell \neq i\}$; and $\mathcal{L}_{Ti} = \{k \in \mathcal{A}^{p,d} : k_i > 0\}$.

4. Assessment of aPCE-based method using MCS

A numerical truss bridge is used as the test-bed to validate the feasibility of the proposed aPCE-based UQ and variance-based GSA method in structural dynamics. As shown in Fig. 2, this truss bridge is 72 m long, 10 m wide, and 16 m high. The truss components, including main chords, struts between top and bottom chords, horizontal and lateral bracings connecting the main chords are all made of steel beams with I-shaped cross section, while the bridge deck, which is supported on the two main girders and five cross girders at an interval of 12 m, is made of concrete. A total of five uncertain parameters are assumed for this numerical truss bridge. The specifications of parameter uncertainties are given in Table 1, in which the means are their nominal values and the coefficient of variation (COV) is the ratio of the standard deviation to the mean. The selection of uncertain parameters' probability distributions should reflect the judgment of how plausible it is that the parameters have certain values. Although the specifications of uncertain parameters associated with this truss bridge are somewhat subjective, it does not violate the purpose of the assessment of the aPCE-based method.

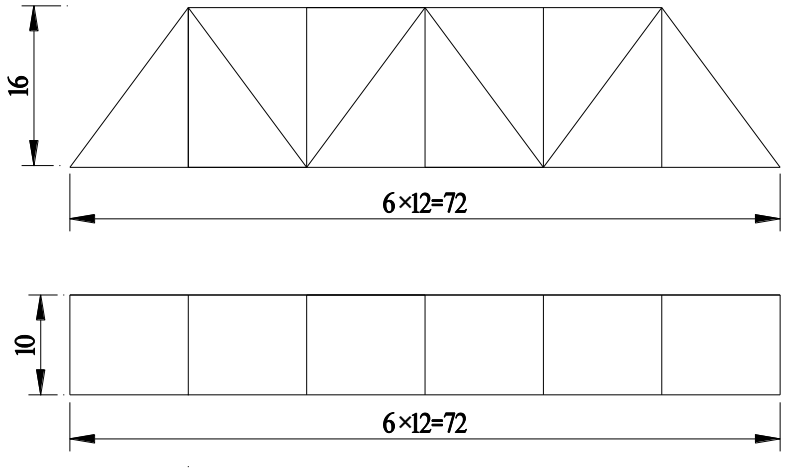

Figure 2. Configuration of truss bridge (unit: m)

Table 1. List of uncertain parameters associated with the truss bridge.

Parameter	Distribution	Mean	COV
Elastic moduli of steel truss frame (E_s)	Lognormal	2.1e11 (Pa)	0.15
Density of steel truss frame (ρ_s)	Weibull	7850 (kg/m^3)	0.10
Elastic moduli of concrete deck (E_c)	Lognormal	3.5e10 (Pa)	0.15
Density of concrete deck (ρ_c)	Weibull	2500 (kg/m^3)	0.10
Thickness of concrete deck (T)	Uniform	0.3 (m)	0.10

The finite element (FE) model and the first four vibration modes of the truss bridge are shown in Fig. 3. The FE model is built using general-purpose mathematical software MATLAB. The natural frequencies and mode shapes are extracted through eigenvalue analysis using *eig* function in MATLAB. Four natural frequencies of the truss bridge corresponding to the mode shapes in Fig. 3 are under consideration. Second-order PCE is usually sufficient to maintain good accuracy for engineering applications [57, 58]. Thus, the model order of the aPCE is set to 2, that is, r=2. For computer experiment, the initial number of training data points is commonly set to 10d (d=5 is the number of model inputs) based on the well-known "n=10d" rule of thumb [59, 60]. Herein, a larger the training data size of 20d is adopted to construct reliable aPCE. Thus, a total of 100 evaluations of FE model are performed for preparing the training data. In summary, the mode order (r) is set

to 2 and the training data size (n) is set to 100 for construction of the aPCE. In the following, the LOOCV procedure is performed for model validation. The measure criterion Q^2's of four aPCEs are 0.9999, 0.9989, 0.9988, and 0.9999, which are larger than the threshold of 0.95. It is verified that the built aPCEs own good prediction performance. It is worth mentioning that when the target systems involve great complexity and strong nonlinearity (e.g., with oscillatory response), it should increase the model order (r) of the aPCE to ensure its modeling flexibility and prediction power. However, the number of the aPCE terms will grow exponentially as model order increases (the well-known as "curse of dimensionality"), which requires a large number of model evaluations (i.e., the computational cost) for determination of aPCE. Fortunately, the sparse grid and/or adaptive schemes can provide an effective remedy to alleviate the "curse of dimensionality" [54, 61].

Subsequently, the constructed aPCEs are adopted to perform UQ and variance-based GSA of the target natural frequencies in a combined manner. The feasibility of the aPCE-based approach is verified by the brute-force MCS. Note that the truss bridge is used here for methodology assessment mainly because that its FE model is quite computationally cheap, which makes the direct parameter-sampled MCS affordable and feasible. A large sample size (i.e., 100,000) for MCS is adopted to ensure the convergence of the UQ and variance-based GSA results. For performing MCS-based implementation of GSA, the least total number is $N(d+2)$ [62], where N is the sample size and d is the number of inputs, so the resultant total number of model evaluation is 700,000.

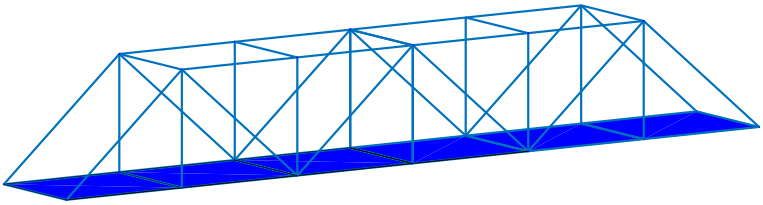

(a) FE model

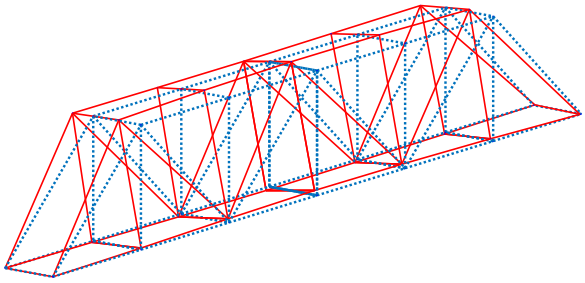

(b) First-order vibration mode

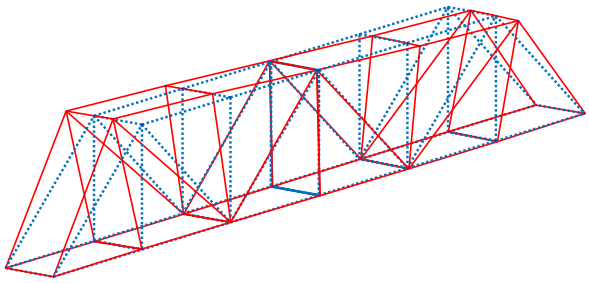

(d) Second-order vibration mode

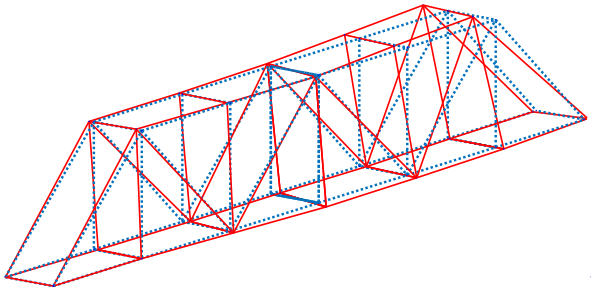

(d) Third-order vibration mode

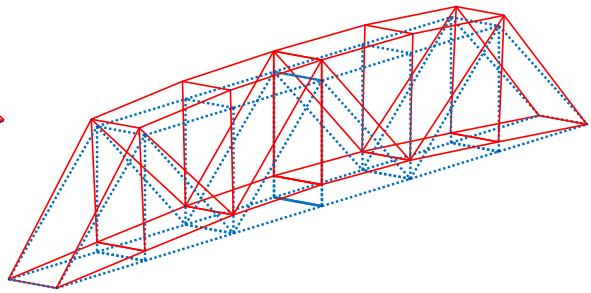

(e) Fourth-order vibration mode

Figure 3. FE model and vibration modes of truss bridge with nominal parameters.

Based on the theory described in Section 3.1, the moments and PDFs of the target natural frequencies can be estimated using the aPCE-based method. Specially, the aPCE surrogate model is used to map the relationship between the uncertain parameters and the natural frequencies, and one aPCE model is constructed for each natural frequency separately. Once the aPCE models are achieved, the moments of natural frequencies can be analytically calculated by simply post-processing the aPCE coefficients and moments of uncertain parameters. As reported in [63], when the first four moments are taken as the prior information about the unknown probability distribution, the MEP technique is able to well characterize the PDF of a random variable. In this regard, only the first four moments are calculated in this paper. The moments of natural frequencies obtained by the aPCE-based method are shown in Fig. 4, and the MEP-derived PDFs estimated from the obtained

moments are shown in Fig. 5. For comparison purpose, the moments and PDFs of natural frequencies calculated by the crude MCS estimator are demonstrated together. As seen from Figs. 4 and 5, the aPCE-derived moments and PDFs have a perfect match with the brute-force MCS-derived counterparts, which verifies the high capability of the proposed aPCE-based method for UQ in structural dynamics.

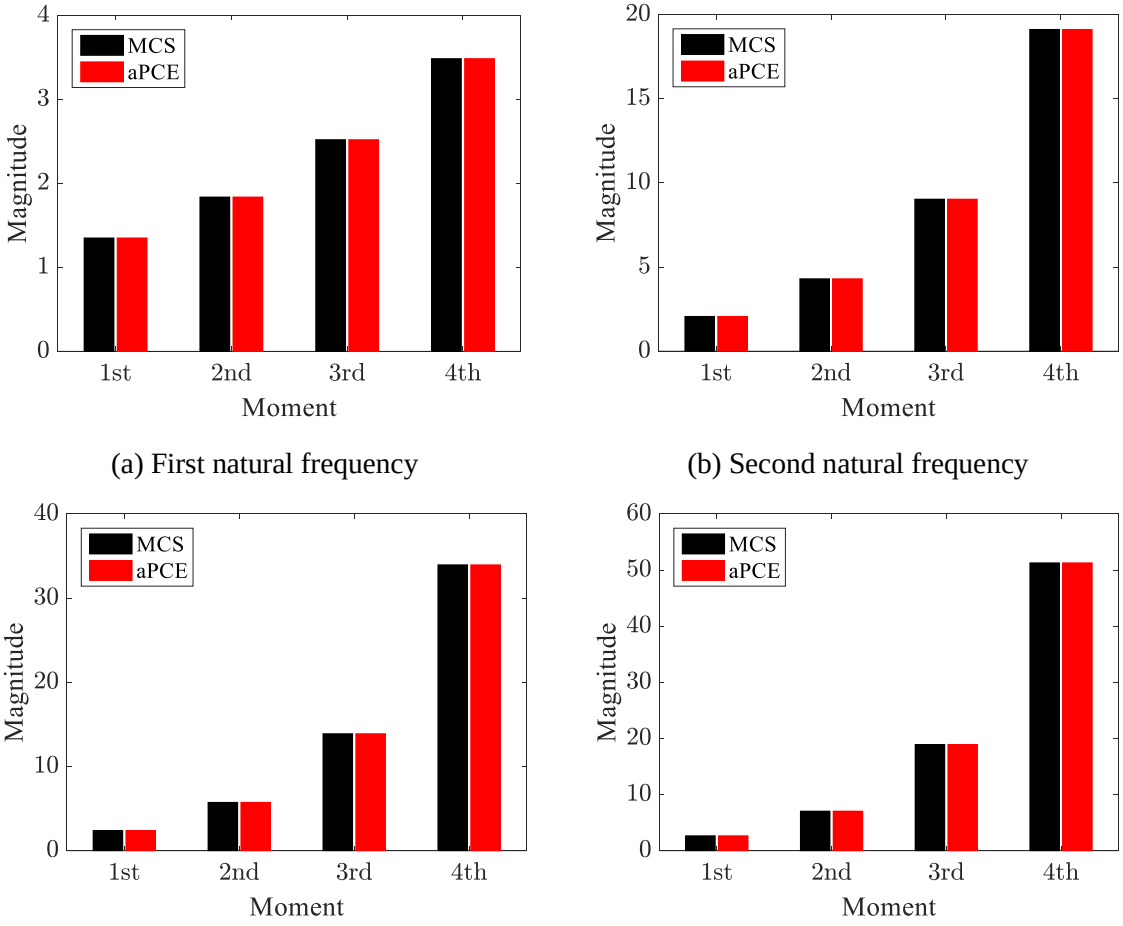

(a) First natural frequency

(b) Second natural frequency

(c) Third natural frequency

(d) Fourth natural frequency

Figure 4. Estimation of statistical characteristics by MCS and aPCE

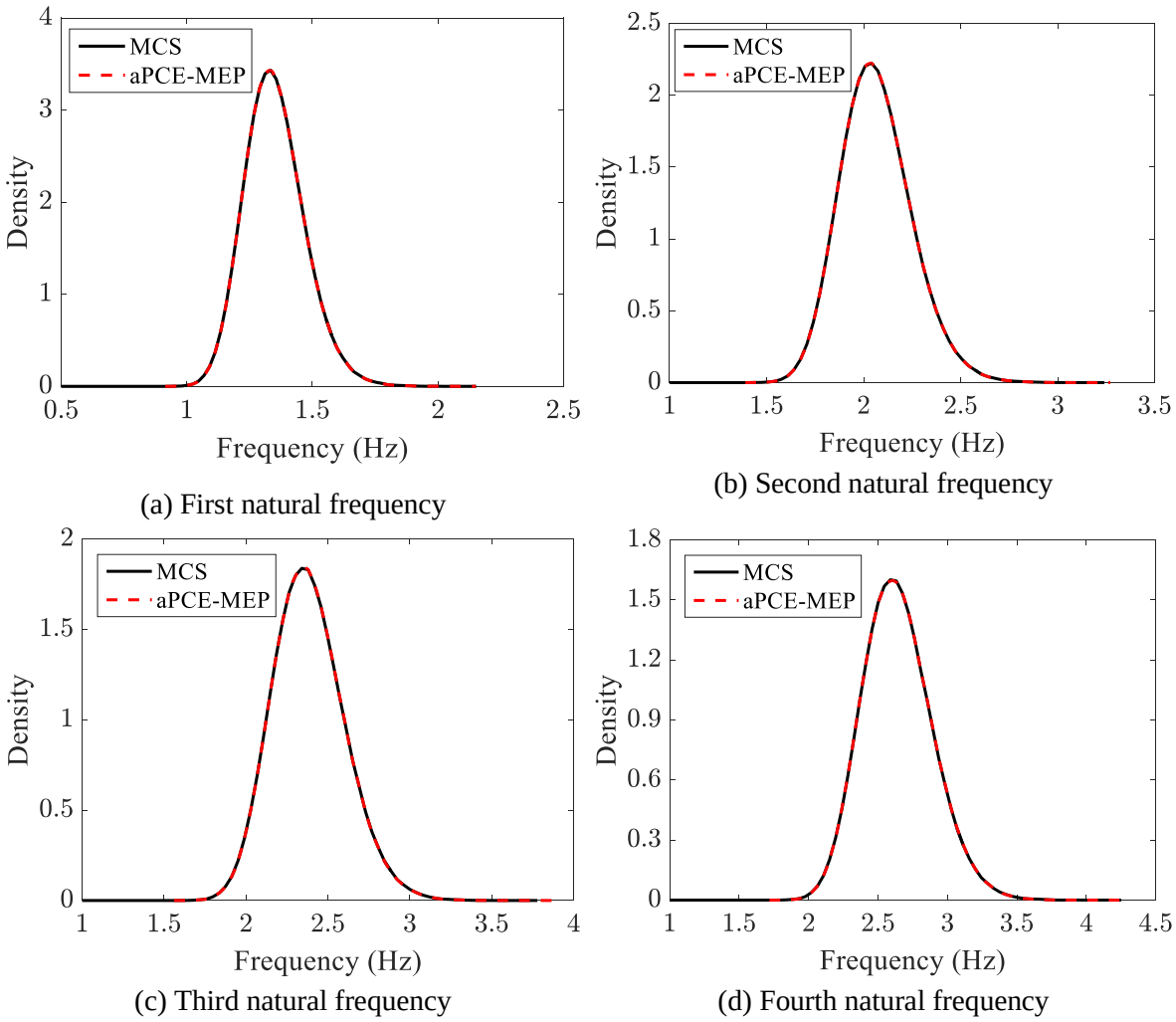

(a) First natural frequency

(b) Second natural frequency

(c) Third natural frequency

(d) Fourth natural frequency

Figure 5. Estimation of probability density by MCS and aPCE-MEP

Having validated the effectiveness of the aPCE-based method in performing UQ, the next agendum is to evaluate its performance for variance-based GSA. Similar to the calculations of moments, the variance-based sensitivity indices can also be analytically computed by simply post-processing the aPCE coefficients, as expressed by Eqs. (50) and (51). Likewise, the direct MCS is employed to verify the accuracy of the aPCE-based approach in conducting GSA. The comparison of the aPCE- and MCS-derived sensitivity indices is provided in Fig. 6, from which one can see that the aPCE-derived sensitivity indices are in close agreement with the MCS-derived counterparts. Therefore, it can be concluded that the proposed aPCE-based method is also reliable for variance-based GSA.

In addition to investigation on the accuracy of the aPCE method for UQ and variance-based GSA, its computational efficiency is also of our concern. The implementations of UQ and variance-based GSA are conducted on a Dell PowerEdge T420 machine with Dual Intel Xeon E5-2403V2 processor and 16 GB memory. The MCS procedure takes around 8 hours and 45 minutes, while the computational time of the aPCE-based estimator is less than 1 minute. In terms of the computational cost, the aPCE method owns an overwhelming superiority over the brute-force MCS. For this simple numerical truss bridge, its FE model is extremely computationally-efficient such that a single run takes about 0.045 sec. Consequently, the computational time of the brute-force MCS is affordable. In practice, the large-scale, complex structures are usually under investigation, and as a result, the direct MCS can become extremely expensive and unaffordable. Assume that a single FE model evaluation takes 1 minute, and then the resultant computational time of the brute-force MCS with 700,000 samples will be around 486 days. In summary, it can be concluded from the comparison results that the aPCE-based approach is highly accurate and computationally efficient for UQ and variance-based GSA in structural dynamics.

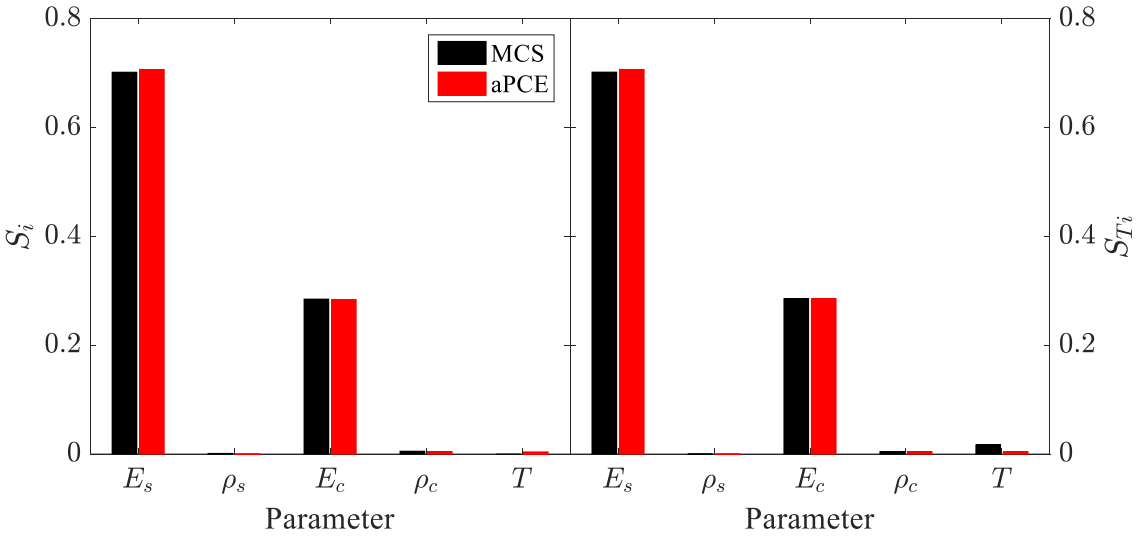

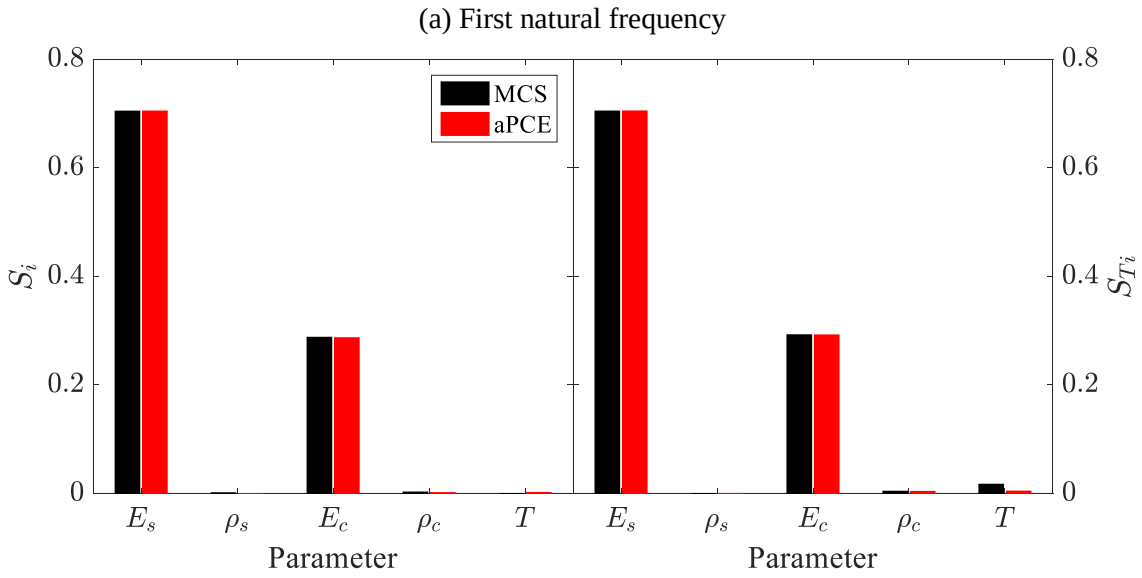

(a) First natural frequency

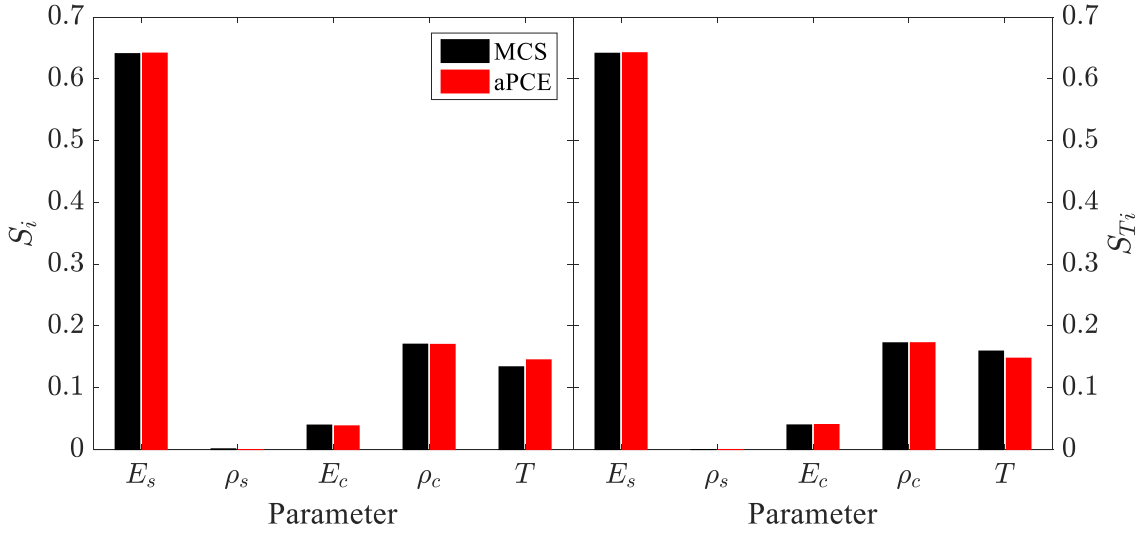

(b) Second natural frequency

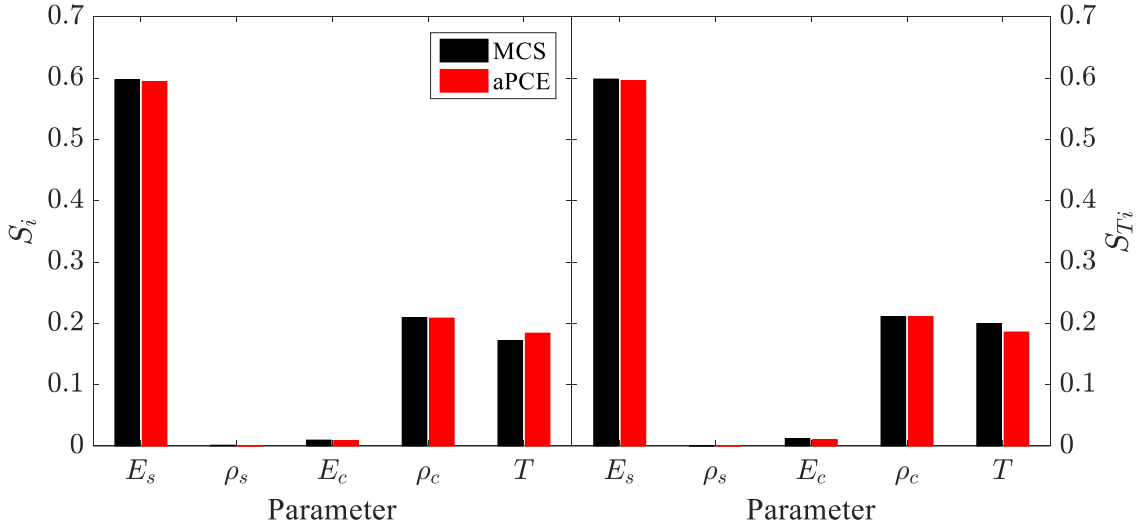

(c) Third natural frequency

(d) Fourth natural frequency

Figure 6. Estimation of sensitivity indices by MCS and aPCE

5. Application: A long-span steel arch bridge

5.1. Bridge description

The Second Hengqin Bridge under investigation is a half-through steel truss arch bridge, located in the city of Zhuhai of Guangdong province of China. This steel truss arch bridge is 600 m long, with a main span of 400 m and two identical side spans of 100 m. The bridge with a total width of 37.2 m is designed to have six traffic lanes. This truss arch bridge with 90-m-high arch ribs becomes the China's longest and widest steel truss arch highway bridge. Fig. 7 shows the configuration of the long-span truss arch bridge.

The superstructure of this truss arch bridge is comprised of two main arch ribs, lateral bracing system, suspenders, and floor system. The main arch ribs have a center-to-center distance of 36 m; and the panel height of the arch ribs ranges from 11 m at the pier to 7 m at the midpoint of the bridge and their panel lengths are also distinct with three different scenarios, specifically 12 m mainly at central span, 16 m mainly at side spans, and 14 m in between. Both top and bottom chords are with box-shaped cross sections. The size of top chords is changing from 1.2 m $\times$ 1.2 m at the arch foot to 1.2 m $\times$ 1.8 m at the arch dome, with thickness between 20 mm and 50 mm, and the size of bottom chords are varying from 1.2 m $\times$ 1.2 m to 1.8 m $\times$ 2.5 m, corresponding to thicknesses of 28 mm and 56 mm, respectively. The deck system consists of main girders, stringers, cross girders, and concrete slab. The arch ribs and the deck are vertically connected through a total of 54 suspenders, which are made of a number of high-strength parallel wire strands.

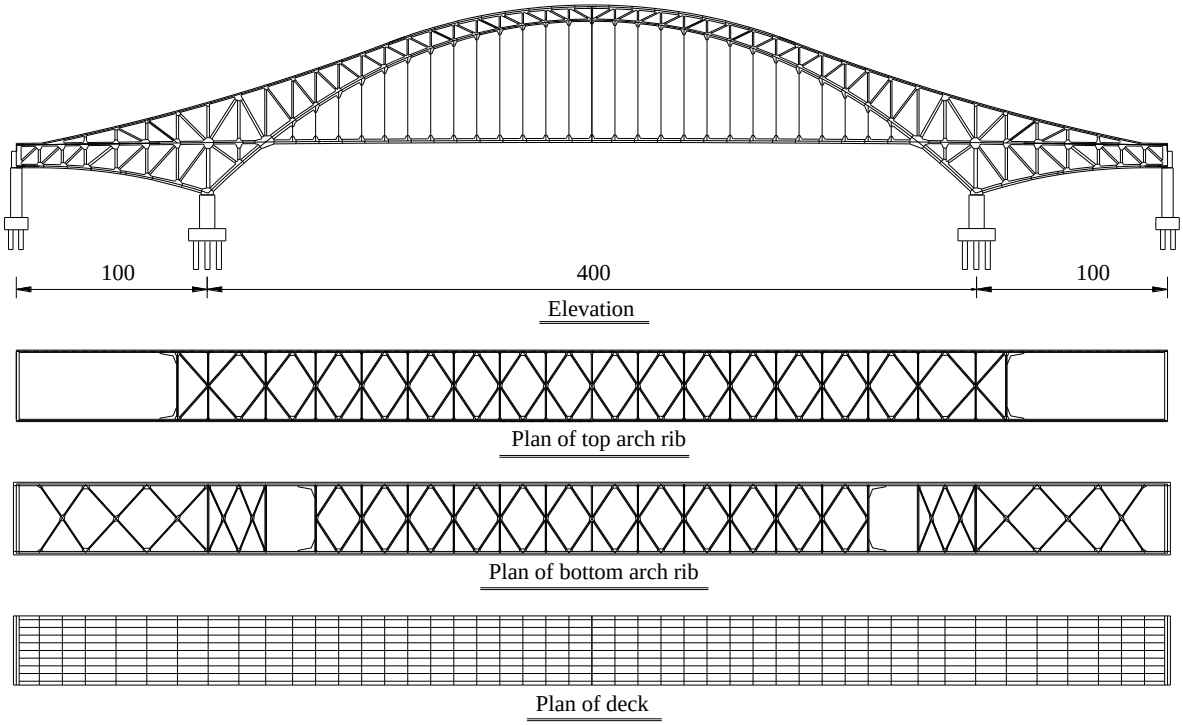

Figure 7. Configuration of Second Hengqin Bridge (unit: m).

5.2. Finite element modeling

The three-dimensional FE model of the Second Hengqin Bridge is built using ANSYS package. The arch ribs, main girders, stringers, cross girders, and lateral bracing are modeled based on their actual cross-sectional properties by using 3D beam elements (BEAM188), which is good at simulating the beam with the variable cross-section. The 3D tension-only truss elements (LINK10) are used to model all suspenders and pre-stressed tie bars. The bridge slab is modeled using the shell elements (SHELL63). In summary, the constructed FE model has a total of 2352 nodes and 2039 elements, including 1615 beam elements, 368 shell elements, and 56 link elements. The resultant FE model and the first vertical and torsional vibration modes of the bridge are demonstrated in Fig. 8.

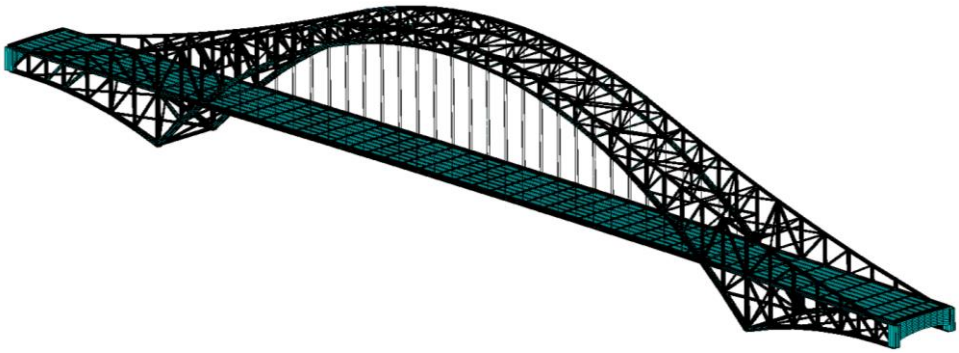

(a) FE model

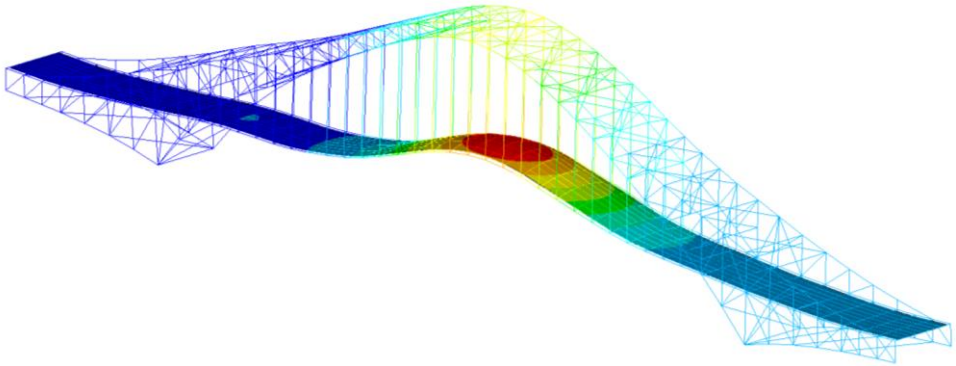

(b) First vertical mode

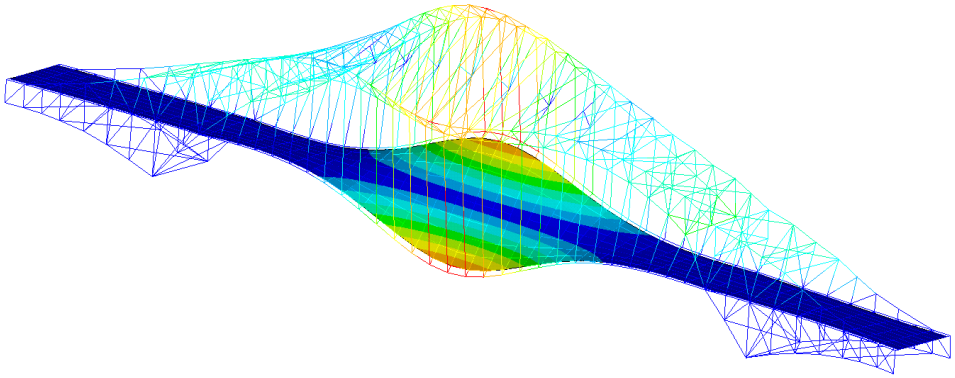

(c) First torsional mode

Figure 8. FE model and vibration modes of Second Hengqin Bridge.

5.3. UQ and variance-based GSA of dynamic characteristics

Uncertainty is ubiquitous in a variety of complex systems. For this long-span truss arch bridge, a total of 11 parameters of five structural components, including girders, arch ribs, lateral bracing, suspenders, and bridge deck, are selected as uncertain variables. The statistical characteristics of these random variables are given in Table 2. The choice of the probability distributions for the parameters is based on the references given in the last

column, and the chosen probability distributions are able to guarantee the positive definiteness of structural properties.

Table 2. Characteristics of uncertain parameters of Second Hengqin Bridge.

Parameter	Distribution	Mean	COV	Source
Elastic modulus of girder (E_g)	Lognormal	2.10e11 (Pa)	0.10	[7, 64]
Density of girder (D_g)	Weibull	7850 (kg/m^3)	0.10	[25, 49]
Elastic modulus of arch rib (E_r)	Lognormal	2.10e11 (Pa)	0.10	[7, 64]
Density of arch rib (D_r)	Weibull	7850 (kg/m^3)	0.10	[25, 49]
Elastic modulus of lateral bracing (E_b)	Lognormal	2.10e11 (Pa)	0.10	[7, 64]
Density of lateral bracing (D_b)	Weibull	7850 (kg/m^3)	0.10	[25, 49]
Elastic modulus of suspender (E_s)	Lognormal	2.05e11 (Pa)	0.10	[7, 64]
Density of suspender (D_s)	Weibull	8680 (kg/m^3)	0.10	[25, 49]
Elastic modulus of deck (E_d)	Lognormal	3.60e10 (Pa)	0.10	[7, 64]
Density of bridge deck (D_d)	Weibull	2600 (kg/m^3)	0.10	[25, 49]
Tickness of bridge (T_d)	Uniform	0.40 (m)	0.10	[25, 65]

Our target dynamic characteristics are the first vertical and torsional natural frequencies corresponding to the mode shapes shown in Fig. 8. To construct the aPCE for each natural frequency, we need a small set of training data generated by performing FE analysis of the original model. Herein, Sobol sequence sampling method, which owns an attractive space-filling feature, is used to generate input samples in terms of parameter probability distributions; and then FE analysis is conducted repeatedly to collect the dynamic characteristics at each sample point. Likewise, the training data size (n) is set to 20d (220) and the mode order (r) is set to 2. The Q^2's of two aPCEs are 0.9998 and 0.9633, larger than the threshold of 0.95, which indicates that the constructed aPCEs are reliable. Once the aPCE surrogate modes are built, the moments of natural frequencies can be analytically calculated. The first four moments of natural frequencies are computed since they are enough for the MEP method for accurate characterization of the probability

distribution of a random variable [63]. The results of the aPCE-derived moments of the natural frequencies are exhibited in Fig. 9. The probability distributions of the natural frequencies are then estimated by the MEP approach based on the obtained moments, and the results are shown in Fig. 10. The attained probability distributions can be used to fully describe the uncertainty and variability existing in the natural frequencies arising from the parameter uncertainty.

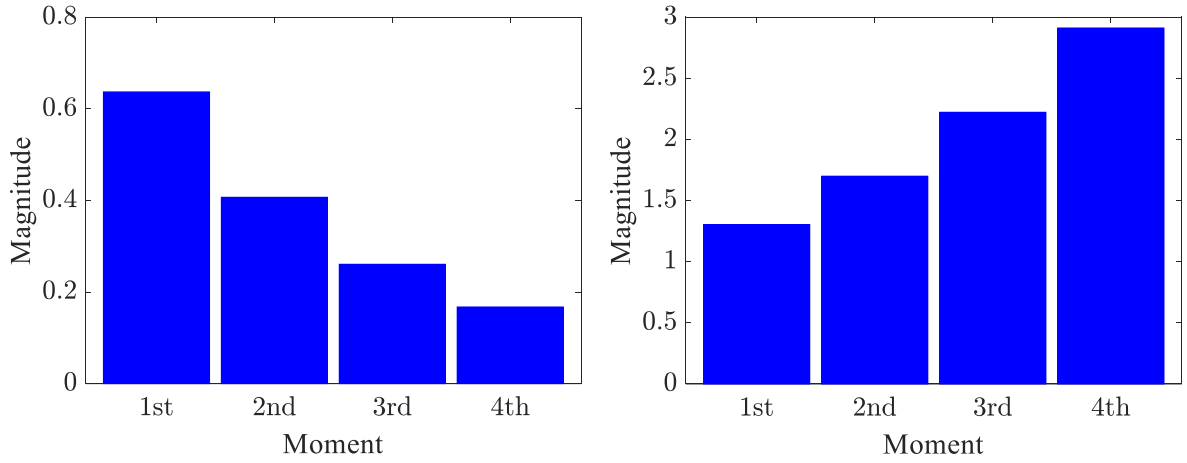

(a) First vertical natural frequency (b) First torsional natural frequency

Figure 9. Statistical characteristics of natural frequencies of Second Hengqin Bridge.

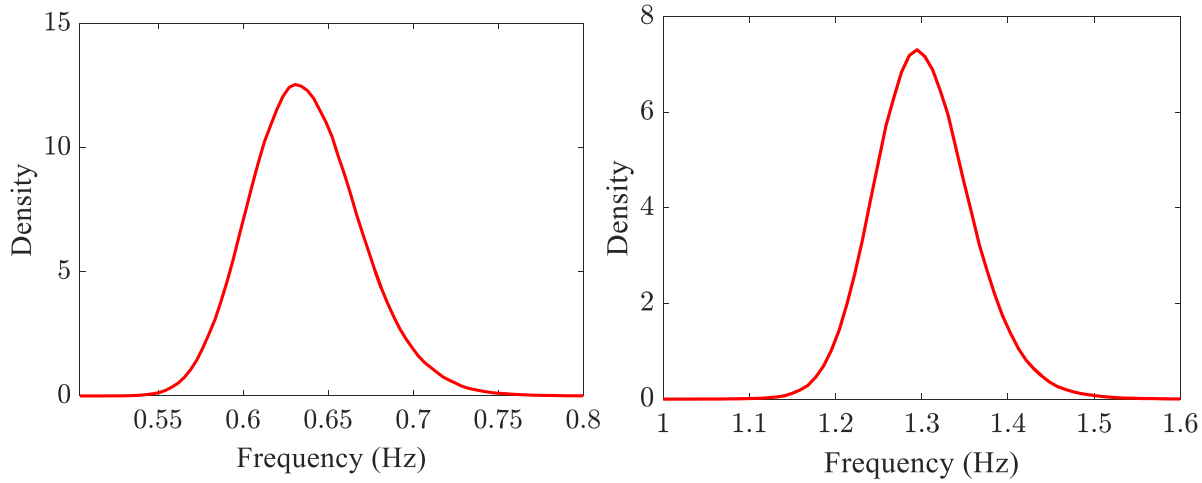

(a) First vertical natural frequency (b) First torsional natural frequency

Figure 10. Probability distributions of natural frequencies of Second Hengqin Bridge.

Following the UQ process, we move on to the investigation on quantification of the contributions of individual parameters to the total uncertainty in natural frequencies, that is,

performing variance-based GSA. The variance-based GSA results associated with the natural frequencies are given in Fig. 11, from which the observations are reported as follows:

- For the first vertical natural frequency, the effects of the parameters E_r, D_d, and T_d are most influential, which means that their uncertainties largely dominate the variation of natural frequency; the parameters E_g, D_g, D_r, E_s, and E_d are slightly sensitive; the remaining parameters are almost insensitive. It is interesting to note that the interaction effects among these parameters on this natural frequency are slight since the discrepancy between their first-order sensitivity indices (S_i) and total ones (S_{Ti}) is almost identical.
- For the first torsional natural frequency, the parameters E_r and D_d present the most significant influences; the parameters E_g, D_g, D_r, and T_d are second most influential, followed by the parameters E_b and E_s; the rest are non-influential. Unlike the previous the first vertical natural frequencies, the mutual effects among parameters are pronounced, which is confirmed by the fact that the total sensitivity indices are larger than the first-order ones. The phenomenon that the interaction affections do account for the certain amount of contributions to the variation of this natural frequency may be illustrated by the corresponding torsional vibration mode shown in Fig. 8, in which one will find that the vibrations of more structural components are excited.
- Combined with the variance-based GSA results and the vibration modes, it may be concluded that if the structural component is largely excited by certain vibration mode, its relevant parameters will be more influential. Specifically, for both vertical and torsional modes, the arch ribs and bridge deck are significantly excited, so their

parameters E_r, D_d, and T_d are influential. The reason why more structural parameters become sensitive for the torsional natural frequency is that the vibrations of more structural components are excited by this torsional vibration mode.

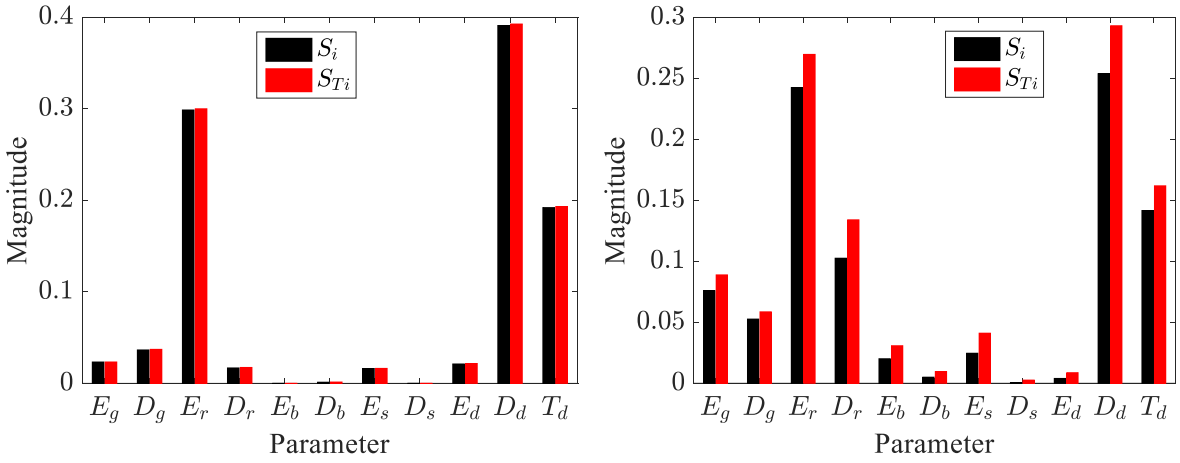

(a) First vertical natural frequency (b) First torsional natural frequency

Figure 11. Sensitivity indices of uncertain parameters of Second Hengqin Bridge.

6. Conclusions

An approach based on the aPCE surrogate model is presented for analytical, unified implementation of UQ and variance-based GSA in structural dynamics of complex structures. The aPCE is employed as a fast-to-run surrogate model of the expensive FE model; and then within the aPCE framework, the UQ and variance-based GSA of dynamic characteristics are achieved in an analytical manner. To be specific, analytical implementation of UQ consists of two stages: the aPCE surrogate model is used for analytical calculation of moments of dynamic characteristics; and then taking the obtained moments as the constraints, the MEP technique is put forth to derive the closed-form expressions of the probability distributions of dynamic characteristics. For variance-based GSA, the analytical computation of the variance-based sensitivity indices is readily achieved by simply post-processing the aPCE coefficients. The aPCE-based approach is

generally suitable for analytical implementation of the UQ and variance-based GSA of dynamic characteristics of complex systems whose parameters can follow arbitrary probability distributions. The effectiveness of the aPCE-based UQ and variance-based GSA approach is verified by the crude parameter-sampled MCS estimator.

A long-span steel truss arch bridge is provided to illustrate the application of the aPCE-based approach to UQ and variance-based GSA in structural dynamics. Based on the aPCE-derived UQ results, we can have a clear picture of how the structural dynamic characteristics are distributed under the parameter uncertainty. Variance-based GSA, which naturally follows UQ as it evaluates how variations of dynamic characteristics can be apportioned quantitatively to different uncertain structural parameters, is performed subsequently. The variance-based GSA results enable us to have a good understanding of how uncertain parameters influence the dynamic characteristics as well as their quantitative contributions to the resultant variations of the dynamic characteristics. In light of the variance-based GSA results, some interesting findings are obtained: (1) the sensitivity of different natural frequencies to structural parameters is different, for example, the parameter D_r has considerable influence on the torsional natural frequency but not on the vertical natural frequency; (2) certain parameters always show great sensitivity to both vertical and torsional natural frequencies, such as the parameters E_r, D_d, and T_d; and (3) the interaction effects among parameters on the different natural frequencies are various, specifically obvious for the torsional natural frequency but not for the vertical one, which may be illustrated by their vibration modes. The present aPCE-based UQ and variance-based GSA approach is very applicable for the large-scale, complex structures with arbitrary probability distributed random parameters since the aPCE-based method enables

589 analytical implementation of UQ and variance-based GSA, and thus is highly
590 computationally efficient.

591 Acknowledgements

592 This research was financially supported by the National Key Research and
593 Development Program of China (2017YFC0806100), the National Natural Science
594 Foundation of China (51878235 and 51778204), and Shenzhen Science and Technology
595 program (KQTD20180412181337494).

Appendix A: Fejér Type-2 rules

Fejér Type-2 rules are nearly identical to Clenshaw-Curtis rules. The only difference is that the Fejér Type-2 rules omit the endpoints ± 1 and are thus open-ended. The explicit expressions for the nodes and the weights of the Fejér Type-2 rules are summarized by Davis and Rabinowitz [66]. The Fejér Type-2 nodes and weights are expressed by [66]

$$\begin{cases} z_i = \cos\left(i\pi/(n+1)\right) \\ q_i = \dfrac{4\sin\left(i\pi/(n+1)\right)}{n+1} \displaystyle\sum_{j=1}^{\lfloor (n+1)/2 \rfloor} \frac{\sin\left((2j-1)i\pi/(n+1)\right)}{2j-1}, \end{cases} \qquad i = 1, 2, \ldots, n \tag{A.1}$$

where $\lfloor \bullet \rfloor$ is the greatest integer function, returning the nearest integer less than or equal to $\bullet$.

Appendix B: Analytical moments of univariate probability distributions

Analytical moments of some commonly-used standard probability distributions are presented in this appendix. A total of six types of probability distributions, that is, uniform, normal, log-normal, beta, gamma, and Weibull, are shown. Note that it does not mean that other probability distributions not mentioned here do not have closed-form expressions of the moments. The moments of these probability distributions are listed in the following table.

611 Table A. Analytical moments of univariate probability distributions.

Distribution	PDF	k -th moment
Uniform	$\frac{1}{u-l}$	$\mathbb{E}(x^k)=\frac{u^{k+1}-l^{k+1}}{(u-l)(k+1)}$
Normal	$\frac{1}{\sigma\sqrt{2\pi}}e^{-\frac{(x-\mu)^2}{2\sigma^2}}$	$\mathbb{E}(x^k)=\sum_{m=0}^{k}\binom{k}{m}\mu^m\sigma^{k-m}g(k-m)$ $g(k-m)=\begin{cases}\frac{(k-m)!}{2^{(k-m)/2}\left((k-m)/2\right)!}, & (k-m)\text{=even}\\ 0, & (k-m)\text{=odd}\end{cases}$
Lognormal	$\frac{1}{x\sigma\sqrt{2\pi}}e^{-\frac{(\ln x-\mu)^2}{2\sigma^2}}$	$\mathbb{E}(x^k)=e^{k(2\mu+k\sigma^2)/2}$
Beta	$\frac{\Gamma(\alpha+\beta)}{\Gamma(\alpha)\Gamma(\beta)}x^{\alpha-1}(1-x)^{\beta-1}$	$\mathbb{E}(x^k)=\frac{\Gamma(\alpha+\beta)\Gamma(\alpha+k)}{\Gamma(\alpha)\Gamma(\alpha+\beta+k)}$
Gamma	$\frac{1}{\Gamma(\alpha)\beta^\alpha}x^{\alpha-1}e^{-\frac{x}{\beta}}$	$\mathbb{E}(x^k)=\frac{\beta^k\Gamma(\alpha+k)}{\Gamma(\alpha)}$
Weibull	$\frac{\alpha}{\beta}\left(\frac{x}{\beta}\right)^{\alpha-1}e^{-\left(\frac{x}{\beta}\right)^\alpha}$	$\mathbb{E}(x^k)=\beta^k\Gamma\left(\frac{\alpha+k}{\alpha}\right)$

612

References

[1] Székely G S, Schuëller G I. Computational procedure for a fast calculation of eigenvectors and eigenvalues of structures with random properties. Computer Methods in Applied Mechanics and Engineering, 2001, 191(8-10):799-816.

[2] Parry G W. The characterization of uncertainty in probabilistic risk assessments of complex systems. Reliability Engineering & System Safety, 1996, 54(2-3): 119-126.

[3] Mace B R, Worden K, Manson G (Editors). Uncertainty in structural dynamics, Journal of Sound and Vibration, 2005, 288 (3):431-790 (Special issue).

[4] Moens D (Editors). Uncertainties in structural dynamics. Mechanical Systems and Signal Processing, 2012, 32:1-4790 (Special issue).

[5] Helton J C, Johnson J D, Sallaberry C J, Storlie C B. Survey of sampling-based methods for uncertainty and sensitivity analysis. Reliability Engineering & System Safety, 2006, 91(10-11):1175-1209.

[6] Ghanem R G, Spanos P D. Stochastic Finite Element Method: Response Statistics. Stochastic finite elements: a spectral approach. Springer, New York, NY, 1991.

[7] Stefanou G. The stochastic finite element method: past, present and future. Computer Methods in Applied Mechanics and Engineering, 2009, 198(9-12):1031-1051.

[8] Adhikari S. Joint statistics of natural frequencies of stochastic dynamic systems. Computational Mechanics, 2007, 40(4):739-752.

[9] Chen S H, Ma L, Meng G W, Guo R. An efficient method for evaluating the natural frequencies of structures with uncertain-but-bounded parameters. Computers & Structures, 2009, 87(9-10):582-590

635 [10]Qiu Z P, Elishakoff I. Antioptimization of structures with large
636 uncertain-but-non-random parameters via interval analysis. Computer methods in
637 applied mechanics and engineering, 1998, 152(3-4):361-372.
638 [11]Chen S H, Ma L, Meng G W, Guo R. An efficient method for evaluating the natural
639 frequencies of structures with uncertain-but-bounded parameters. Computers &
640 Structures, 2009, 87(9-10):582-590.
641 [12]Gao W. Natural frequency and mode shape analysis of structures with uncertainty.
642 Mechanical Systems and Signal Processing, 2007, 21(1):24-39.
643 [13]Moens D, Vandepitte D. Interval sensitivity theory and its application to frequency
644 response envelope analysis of uncertain structures. Computer Methods in Applied
645 Mechanics and Engineering, 2007, 196(21-24):2486-2496.
646 [14]Ghanem R, Ghosh D. Efficient characterization of the random eigenvalue problem in a
647 polynomial chaos decomposition. International Journal for Numerical Methods in
648 Engineering, 2007, 72(4):486-504.
649 [15]Chowdhury R, Adhikari S. High dimensional model representation for stochastic finite
650 element analysis. Applied Mathematical Modelling, 2010, 34(12):3917-3932.
651 [16]DiazDelaO F A, Adhikari S, Saavedra Flores E I, Friswell M I. Stochastic structural
652 dynamic analysis using Bayesian emulators. Computers & Structures, 2013, 120:24-32.
653 [17]Wan H P, Mao Z, Todd M D, Ren W X. Analytical uncertainty quantification for modal
654 frequencies with structural parameter uncertainty using a Gaussian process metamodel.
655 Engineering Structures, 2014, 75:577-589.

[18]Xia Z, Tang J. Characterization of dynamic response of structures with uncertainty by using Gaussian processes. Journal of Vibration and Acoustics, 2013, 135(5):051006-051006.

[19]Zhou K, Tang J. Uncertainty quantification in structural dynamic analysis using two-level Gaussian processes and Bayesian inference. Journal of Sound and Vibration, 2018, 412:95-115.

[20]Su L, Wan H P, Dong Y, Frangopol D M, Ling X Z. Efficient uncertainty quantification of wharf structures under seismic scenarios using Gaussian process surrogate model. Journal of Earthquake Engineering, 2018:1-22.

[21]Wei X, Wan H P, Russell J, Živanović S, He X. Influence of mechanical uncertainties on dynamic responses of a full-scale all-FRP footbridge. Composite Structures, 2019, 223, 110964.

[22]Pradlwarter H J, Schuëller G I. On advanced Monte Carlo simulation procedures in stochastic structural dynamics. International Journal of Non-Linear Mechanics, 1997, 32(4):735-744.

[23]Song D, Chen S, Qiu Z. Stochastic sensitivity analysis of eigenvalues and eigenvectors. Computers & structures, 1995, 54(5):891-896.

[24]Chowdhury R, Adhikari S. Stochastic sensitivity analysis using preconditioning approach. Engineering Computations, 2010, 27(7): 841-862.

[25]Wan H P, Todd M D, Ren W X. Statistical framework for sensitivity analysis of structural dynamic characteristics. Journal of Engineering Mechanics, 2017, 143(9):04017093.

678 [26]Saltelli A, Andres T, Campolongo F, Cariboni J, Gatelli D, Ratto M, Saisana M,
679 Tarantola S. Global sensitivity analysis the primer. John Wiley & Sons, 2008.
680 [27]Wan H P, Ren W X. Parameter selection in finite element model updating by global
681 sensitivity analysis using Gaussian process metamodel. Journal of Structural
682 Engineering, 2015, 141(6): 04014164.
683 [28]Sobol I M. Sensitivity estimates for nonlinear mathematical models. Mathematical
684 Modeling and Computational Experiment, 1993, 1(4):407-414.
685 [29]Morris M D. Factorial sampling plans for preliminary computational experiments.
686 Technometrics, 1991, 31(2):161-174.
687 [30]Saltelli A, Marivoet J. Non-parametric statistics in sensitivity analysis for model output:
688 a comparison of selected techniques. Reliability Engineering & System Safety, 1990,
689 28(2): 229-253.
690 [31]Wu J, Luo Z, Zhang N, Zhang Y. A new uncertain analysis method and its application
691 in vehicle dynamics. Mechanical Systems and Signal Processing, 2015, 50-51:659-675.
692 [32]Jacquelin E, Adhikari S, Sinou J J, Friswell M I. Polynomial chaos expansion in
693 structural dynamics: Accelerating the convergence of the first two statistical moment
694 sequences. Journal of Sound and Vibration, 2015, 356:144-154.
695 [33]Li K, Gao W, Wu D, Song C, Chen T. Spectral stochastic isogeometric analysis of
696 linear elasticity. Computer Methods in Applied Mechanics and Engineering, 2018,
697 332:157-190.
698 [34]Ni P, Li J, Hao H, Xia Y. Stochastic dynamic analysis of marine risers considering
699 Gaussian system uncertainties. Journal of Sound and Vibration, 2018, 416:224-243.

[35]Ni P, Xia Y, Li J, Hao H. Using polynomial chaos expansion for uncertainty and sensitivity analysis of bridge structures. Mechanical Systems and Signal Processing, 2019, 119, 293-311.

[36]Menga E, Sánchez M J, Romero I, Hernández S. A sample-based approach to estimate the dynamic loads of components with nonlinear uncertain interfaces. Aerospace Science and Technology, 2019, 87: 369-378.

[37]Yuan Z, Liang P, Silva T, Yu K, Mottershead J E. Parameter selection for model updating with global sensitivity analysis. Mechanical Systems and Signal Processing, 2019, 115:483-496.

[38]Wiener N. The homogeneous chaos. American Journal of Mathematics, 1938, 60(4):897-936.

[39]Xiu D, Karniadakis G E. The Wiener-Askey polynomial chaos for stochastic differential equations. SIAM journal on scientific computing, 2002, 24(2):619-644.

[40]Wan X, Karniadakis G E. Beyond wiener-askey expansions: Handling arbitrary PDFs. Journal of Scientific Computing, 2006, 27(1):455-464.

[41]Witteveen J A S, Bijl H. Modeling arbitrary uncertainties using Gram-Schmidt polynomial chaos. 44th AIAA aerospace sciences meeting and exhibit. 2006.

[42]Witteveen J A S, Sarkar S, Bijl H. Modeling physical uncertainties in dynamic stall induced fluid-structure interaction of turbine blades using arbitrary polynomial chaos. Computers & Structures, 2007, 85(11):866-878.

[43]Oladyshkin S, Nowak W. Data-driven uncertainty quantification using the arbitrary polynomial chaos expansion. Reliability Engineering & System Safety, 2012, 106:179-190.

[44]Wan H P, Ren W X, Todd M D. An efficient metamodeling approach for uncertainty quantification of complex systems with arbitrary parameter probability distributions. International Journal for Numerical Methods in Engineering, 2017, 109(5):739-760.

[45]Yin S, Yu D, Luo Z, Xia B. An arbitrary polynomial chaos expansion approach for response analysis of acoustic systems with epistemic uncertainty. Computer Methods in Applied Mechanics and Engineering, 2018, 332:280-302.

[46]Yin S, Yu D, Luo Z, Xia B. Unified polynomial expansion for interval and random response analysis of uncertain structure-acoustic system with arbitrary probability distribution. Computer Methods in Applied Mechanics and Engineering, 2018, 336:260-285.

[47]Crestaux T, Le Ma ître O, Martinez J M. Polynomial chaos expansion for sensitivity analysis. Reliability Engineering & System Safety, 2009, 94(7):1161-1172.

[48]Gautschi W. Orthogonal Polynomials: Computation and Approximation. Oxford University Press: Oxford, 2004.

[49]Rahman S. Extended polynomial dimensional decomposition for arbitrary probability distributions. Journal of Engineering Mechanics, 2009, 135(12):1439-1451.

[50]Gander M J, Karp A H. Stable computation of high order Gauss quadrature rules using discretization for measures in radiation transfer. Journal of Quantitative Spectroscopy and Radiative Transfer, 2001, 68(2):213-223.

[51]Parlett B N. The symmetric eigenvalue problem, Volume 20 of Classics in applied mathematics. Philadelphia, PA: SIAM. 1998.

[52]Gragg W, Harrod W. The numerically stable reconstruction of Jacobi matrices from spectral data. Numerische Mathematik, 1984, 44(3):317-335.

[53]Gautschi W. On generating orthogonal polynomials. SIAM Journal on Scientific and Statistical Computing, 1982, 3(3):289-317.

[54]Blatman G, Sudret B. An adaptive algorithm to build up sparse polynomial chaos expansions for stochastic finite element analysis. Probabilistic Engineering Mechanics, 2010, 25(2): 183-197.

[55]Jaynes E T. Information theory and statistical mechanics. Physical review, 1957, 106(4): 620.

[56]Sudret B. Global sensitivity analysis using polynomial chaos expansions. Reliability Engineering & System Safety, 2008, 93(7):964-979.

[57]Wu S Q, Law S S. Evaluating the response statistics of an uncertain bridge–vehicle system. Mechanical Systems and Signal Processing, 2012, 27:576-589.

[58]Rahman S. Wiener-Hermite polynomial expansion for multivariate Gaussian probability measures. Journal of Mathematical Analysis and Applications, 2017, 454(1): 303-334.

[59]Loeppky J L, Sacks J, Welch W J. Choosing the sample size of a computer experiment: A practical guide. Technometrics, 2009, 51(4): 366-376.

[60]Konakli K, Sudret B. Polynomial meta-models with canonical low-rank approximations: numerical insights and comparison to sparse polynomial chaos expansions. Journal of Computational Physics, 2016, 321: 1144-1169.

[61]Blatman G, Sudret B. Adaptive sparse polynomial chaos expansion based on least angle regression. Journal of Computational Physics, 2011, 230(6):2345-2367.

[62]Tarantola S, Becker W, Zeitz D. A comparison of two sampling methods for global sensitivity analysis. Computer Physics Communications, 2012, 183(5):1061-1072.

768 [63]Sobezyk K, Trębicki J. Maximum entropy principle in stochastic dynamics.
769 Probabilistic Engineering Mechanics, 1990, 5(3):102-110.
770 [64]Zhang H, Ellingwood B R, Rasmussen K J R. System reliabilities in steel structural
771 frame design by inelastic analysis. Engineering Structures, 2014, 81:341-348.
772 [65]Soleimani F, Vidakovic B, DesRoches R, Padgett J. Identification of the significant
773 uncertain parameters in the seismic response of irregular bridges. Engineering
774 Structures, 2017, 141:356-372.
775 [66]Davis P J, Rabinowitz P. Methods of numerical integration. Courier Corporation, 2007.